HHS Public Access

Author manuscript

Neuron. Author manuscript; available in PMC 2019 August 22.

Published in final edited form as:

Neuron. 2018 August 22; 99(4): 842–853.e8. doi:10.1016/j.neuron.2018.07.038.

A dynamic interplay within the frontoparietal network underlies rhythmic spatial attention

Ian C. Fiebelkorn[1,2], **Mark A. Pinsk**[1], and **Sabine Kastner**[1]

[1]Princeton Neuroscience Institute and Department of Psychology, Princeton University, Princeton, NJ 08544, USA.

[2]Lead Contact

SUMMARY

Classic studies of spatial attention assumed that its neural and behavioral effects were continuous over time. Recent behavioral studies have instead revealed that spatial attention leads to alternating periods of heightened or diminished perceptual sensitivity. Yet the neural basis of these rhythmic fluctuations has remained largely unknown. We show that a dynamic interplay within the macaque frontoparietal network accounts for the rhythmic properties of spatial attention. Neural oscillations characterize functional interactions between the frontal eye fields (FEF) and the lateral intraparietal area (LIP), with theta phase (3–8 Hz) coordinating two rhythmically alternating states. The first is defined by FEF-dominated beta-band activity, associated with suppressed attentional shifts, and LIP-dominated gamma-band activity, associated with enhanced visual processing and better behavioral performance. The second is defined by LIP-specific alpha-band activity, associated with attenuated visual processing and worse behavioral performance. Our findings reveal how network-level interactions organize environmental sampling into rhythmic cycles.

eTOC BLURB

Fiebelkorn et al., use simultaneous recordings in two hubs of the macaque frontoparietal network to demonstrate a neural basis of rhythmic sampling during spatial attention. Theta-organized, alternating attentional states, characterized by different spatiotemporal dynamics, shape environmental sampling.

CORRESPONDING AUTHOR Ian C. Fiebelkorn, Princeton Neuroscience Institute, Princeton University, Princeton, NJ 08544, USA, phone: +1-609-258-7767. iancf@princeton.edu.

AUTHOR CONTRIBUTIONS

Conceptualization, I.C.F. and S.K.; Methodology, I.C.F., S.K., and M.A.P.; Investigation, I.C.F. and M.A.P.; Formal Analysis, I.C.F.; Resources, S.K.; Funding Acquisition, S.K. Writing - Original Draft, I.C.F. and S.K.; Writing – Review & Editing, I.C.F., S.K., and M.A.P.

DECLARATION OF INTERESTS

The authors declare no competing interests.

INTRODUCTION

Imagine New York's Times Square: tall buildings, flashing lights, a swarm of people. Given the brain's limited processing resources, this scene represents an overload of sensory information. To overcome its processing limits, the brain uses various filtering mechanisms, broadly referred to as selective attention. Visual-spatial attention, one such mechanism, is instrumental in environmental sampling. It operates by boosting neural processing at behaviorally relevant locations (Moran and Desimone, 1985), thereby improving behavioral outcomes, such as detection rates and reaction times (Posner, 1980). Classic studies likened spatial attention to a sustained spotlight that continuously boosts neural processing during attentional deployment (Posner, 1980). Recent evidence, however, has instead revealed that spatial attention samples the visual environment in rhythmic cycles (Busch and VanRullen, 2010; Dugue et al., 2015; Dugue et al., 2016; Fiebelkorn et al., 2013a; Helfrich et al., 2018; Lakatos et al., 2008; Landau and Fries, 2012; Landau et al., 2015; Song et al., 2014; VanRullen et al., 2007). That is, the metaphorical spotlight of spatial attention blinks, leading to alternating periods of either heightened or diminished perceptual sensitivity.

Much of the evidence for rhythmic sampling during spatial attention (i.e., the blinking spotlight) has come from human behavioral studies (Fiebelkorn et al., 2013a; Landau and Fries, 2012; Song et al., 2014; VanRullen et al., 2007). We recently demonstrated, for example, that spatial attention is associated with theta-rhythmic fluctuations (3–8 Hz) in hit rates (HRs) at the attended location (Fiebelkorn et al., 2013a). While we specifically observed these fluctuations in HRs under conditions of covert spatial attention, theta-band rhythmicity appears to be generally characteristic of environmental sampling. Previous studies have similarly linked theta rhythms to overt sampling routines, such as eye movements in primates (Bosman et al., 2009; Hogendoorn, 2016; Otero-Millan et al., 2008; Wutz et al., 2016) and whisking in rodents (Berg and Kleinfeld, 2003; Fanselow and Nicolelis, 1999). Converging evidence thus indicates that environmental sampling, whether through covert or overt mechanisms, is a fundamentally rhythmic process (Schroeder et al., 2010), with a sampling rate in the theta band.

Importantly, theta-rhythmic fluctuations associated with environmental sampling do not reflect entrainment of neural activity to rhythmic stimulation (Lakatos et al., 2008). That is, they emerge in the absence of external rhythms (Bosman et al., 2009; Busch and VanRullen, 2010; Fanselow and Nicolelis, 1999; Fiebelkorn et al., 2013a; Landau and Fries, 2012), indicating that internally generated rhythms shape environmental sampling. Yet the neural basis of these internally generated rhythms has remained largely unknown. Neurophysiological investigations—MEG in humans (Landau et al., 2015) and intracortical recordings in monkeys (Bosman et al., 2009)—have thus far revealed ties between environmental sampling and theta rhythms in visual cortex. For example, Landau et al. (2015) demonstrated that induced gamma-band activity (30–90 Hz) in human visual cortex fluctuates at a theta rhythm (4 Hz), with theta-linked peaks in this gamma-band activity associated with better visual-target detection. Theta rhythms, however, are not limited to visual cortex, having been extensively studied in multiple brain regions (Colgin, 2013). Perhaps most relevant to investigating the rhythmic properties of environmental sampling, theta rhythms occur in the network of frontal and parietal regions that directs both spatial

attention and eye movements (Phillips et al., 2014; Sellers et al., 2016). Here, we hypothesized that rhythmic sampling during spatial attention stems from neural oscillatory activity in this frontoparietal network.

We first establish behavioral evidence of rhythmic sampling in monkeys, using the same spatial cueing task previously shown to elicit rhythmic sampling in humans (Fig. 1) (Egly et al., 1994; Fiebelkorn et al., 2013a). We then present neurophysiological data from simultaneous recordings in two well-characterized hubs of the macaque frontoparietal network: the frontal eye fields (FEF) (Squire et al., 2013) and the lateral intraparietal area (LIP) (Bisley and Goldberg, 2010) (Fig. S1). Our findings are consistent with theta phase in the frontoparietal network shaping behavioral performance through the coordination of two rhythmically alternating states. The first state is characterized by (i) an FEF-dominated, spatially non-specific boost in beta-band activity (16–35 Hz), associated with suppressed attentional shifts, and (ii) an LIP-dominated, spatially specific boost in gamma-band activity (> 35 Hz), associated with enhanced visual processing and better behavioral performance at the cued location. The second state is characterized by a spatially specific boost in LIP alpha-band activity (9–15 Hz), associated with attenuated visual processing and worse behavioral performance at the cued location. The present results thus reveal that rhythmic sampling during spatial attention is linked to an ongoing, dynamic interplay between hubs of the frontoparietal network.

RESULTS

Behavioral evidence of rhythmic sampling

We trained two monkeys to perform a variant of the Egly-Driver task (Fig. 1) (Egly et al., 1994; Fiebelkorn et al., 2013a), where a peripheral spatial cue indicated the most likely location of a subsequent, low-contrast visual target (78% cue validity). The animals maintained fixation throughout each trial and responded by releasing a lever. Both monkeys demonstrated higher HRs at the cued location relative to an uncued location that was positioned on a second object (averaged across monkeys: HRs: 81.5% as compared to 68.1%, *t* test, $p < 0.0001$; Table S1).

We next examined whether behavioral performance at the attended location varied as a function of the cue-target delay (i.e., when the low-contrast visual target was presented relative to the cue; Fig. 2A). Here, we used the fast Fourier transform (FFT) to measure oscillatory patterns in the behavioral time-series data (Figs. 2B, S2) (Fiebelkorn et al., 2011). Our analyses revealed significant theta-rhythmic fluctuations (3–8 Hz) in HRs at the attended location (Fig. 2B; permutation test, $p < 0.005$; see STAR Methods). These findings mirror our previous behavioral results in humans (Fiebelkorn et al., 2013a), demonstrating that spatial attention in monkeys is likewise associated with alternating periods of either enhanced or diminished perceptual sensitivity. Theta-rhythmic sampling therefore seems to be a fundamental property of spatial attention, having been evolutionarily preserved across at least two primate species.

Rhythms in behavioral data (e.g., Fig. 2) seemingly necessitate a brain source with consistent phase alignment across trials. That is, the observed oscillatory pattern in visual-

target detection suggests a consistent phase reset of behaviorally relevant theta rhythms following the spatial cue. Figure S3 provides evidence of such inter-trial phase consistency (in both FEF and LIP), at low theta frequencies (4–5 Hz), that outlasts the initial cue-evoked change in theta power.

General attention effects in FEF and LIP

All analyses of the neurophysiological data are focused on the time period after the cueevoked response (i.e., the visual-sensory response) and until target onset (i.e., the cue-target delay), during which the animals deployed spatial attention at the cued location and the neural response generally satisfied methodological assumptions of stationarity (see STAR Methods). Figures S4 and S5 confirm the involvement of FEF and LIP in the present task, illustrating spike rates and local field potentials (LFPs) during this cue-target delay.

In FEF and LIP, neurons are typically classified based on their response profiles as visual (i.e., sensory-related responses), visual-movement (i.e., sensory and saccade-related responses), and movement (i.e., saccade-related responses) types (Barash et al., 1991; Bruce and Goldberg, 1985; Gregoriou et al., 2012; Thompson et al., 2005). Given low cell counts for movement neurons (N = 15 in FEF; N = 20 in LIP), the present analyses were limited to visual and visual-movement neurons (see STAR Methods and Figure S6 for a description of how we adopted this neuronal classification despite the absence of task-related saccades, i.e., our monkeys released a lever to indicate the occurrence of a visual target). We recorded from 81 neurons in FEF and 80 neurons in LIP that demonstrated increased spiking activity in response to visual stimulation (i.e., visual and visual-movement neurons). In both FEF and LIP, the population of visually responsive neurons demonstrated significantly increased spiking activity during the cue-target delay (Fig. S4), specific to when receptive fields overlapped the cued location (Wilcoxon rank-sum test, $p < 0.0001$) (Gregoriou et al., 2012; Thompson et al., 2005).

We similarly observed attention-related changes in LFPs during the cue-target delay. Figure S5 shows oscillatory power (from 3–60 Hz), time-locked to target presentation. These spectrograms were averaged across 98 recording sessions in FEF and 97 recording sessions in LIP. In FEF, we observed significant increases in oscillatory power in the beta (24–30 Hz) and gamma bands (36–60 Hz) under conditions of spatial attention (i.e., when response fields overlapped the cued location relative to when response fields instead overlapped the uncued location). In LIP, we observed significant, attention-related increases in oscillatory power in the alpha (12–14 Hz), beta (18–22 Hz and 30–34 Hz), and gamma bands (38–42 and 46–48 Hz). Combined with our analyses of single-unit activity (Fig. S4), these results confirm that FEF and LIP contributed to the maintenance of spatial attention at the cued location.

Behavioral performance and oscillatory neural activity

Neural oscillations are comprised of synchronous, rhythmic shifts between high- and low-excitability states (at the level of neural populations). Here, we investigated whether HRs were specifically dependent on the phase of neural oscillations (from 3–60 Hz) (Fiebelkorn et al., 2013b). Our results revealed a significant relationship between oscillatory phase and

visual-target detection (permutation test, $p < 0.0009$), consistent with rhythmic sampling being linked to neural oscillations in FEF and LIP (Fig. 3A–D, S7). In agreement with our behavioral data (Fig. 2) (Fiebelkorn et al., 2013a), we observed phase-detection relationships in the theta band, with a peak at 5 Hz for FEF and at 4 Hz for LIP. For each cortical region, the data also revealed significant relationships between oscillatory phase and visual-target detection (permutation test, $p < 0.0009$) in the alpha (peaks at 10 and 12 Hz in FEF and LIP, respectively) and beta (peaks at 21 and 28 Hz in FEF and LIP, respectively) bands. For LIP, phase-detection relationships also extended into the lower gamma band (35–40 Hz). Previous findings in humans have only provided evidence of rhythmic sampling at lower frequencies (i.e., < 15 Hz) (Busch and VanRullen, 2010; Fiebelkorn et al., 2013a; Landau and Fries, 2012; VanRullen et al., 2007). In contrast, the present intracortical data, with a better signal-to-noise ratio and better spatiotemporal resolution, demonstrate that higher-frequency oscillations (i.e., > 15 Hz) are also linked to fluctuations in perceptual sensitivity during spatial attention.

We next investigated whether phase-detection relationships at higher frequencies are functionally dependent on, or alternatively, functionally independent from theta-band activity. A functional dependence of higher-frequency activity on theta-band activity would be suggestive of a single sampling process as opposed to multiple, independent sampling processes. We first sorted trials into two bins based on their pre-target theta phase: centered on either (i) the phase associated with relatively good behavioral performance or (ii) the phase associated with relatively poor behavioral performance (Fig. 3A, B). We then generated phase-detection relationships within each theta-phase bin for frequencies from 9–60 Hz (Fig. 3E, F; see STAR Methods) (Fiebelkorn et al., 2013b). For both FEF and LIP, significant phase-detection relationships at higher frequencies occurred almost exclusively during the “good” theta phase (permutation test, $p < 0.001$), with the exception of phase-detection relationships in the alpha band (in LIP), which occurred during the “poor” theta phase. These results are therefore consistent with phase-detection relationships at higher frequencies being yoked to theta-band rhythms, reflecting a single, theta-dependent sampling process. These results also strongly suggest an underlying neural mechanism that might shape that sampling process: crossfrequency phase-amplitude coupling (PAC).

Theta phase coordinates neural activity in the frontoparietal network

Lower- and higher-frequency bands are often linked through a hierarchical organization, with the phase of lower frequencies modulating the amplitude (or power) of higher frequencies (Canolty and Knight, 2010; Jensen and Colgin, 2007). Such cross-frequency PAC is thought to temporally coordinate neural activity associated with cognitive functions (Schroeder and Lakatos, 2009). We hypothesized that PAC between theta phase and higher-frequency power might shape environmental sampling during spatial attention, creating alternating windows where the phase of higher-frequency activity is either linked to behavioral performance (i.e., during the high-power theta phase) or not (i.e., during the low-power theta phase).

Figure 4 (A, B) summarizes the strength of within-region PAC, when either the cued or the uncued location fell within the response fields (i.e., the LFP equivalent of receptive fields;

Fig. S8). For FEF, there was significant PAC between theta phase (from 4–6 Hz) and high-beta/gamma power (at 20–56 Hz), with a peak in the high-beta range (at 31 Hz; permutation test, $p < 0.001$). This effect was not spatially specific, occurring both when response fields overlapped the cued location and when response fields overlapped the uncued location. Comparing across these two conditions (i.e., cued vs. uncued), there was significantly stronger PAC between theta phase and high-beta power (at 30–35 Hz) under conditions of spatial attention (permutation test, $p < 0.001$). In contrast, there was significantly stronger PAC between theta phase and low-beta power (at 13–17 Hz) outside the focus of spatial attention.

For LIP, there was significant PAC between theta phase (at 4–6 Hz) and both beta (at 15–27 Hz) and gamma power (at 32–55 Hz) when response fields overlapped the cued location (permutation test, $p < 0.001$), with peaks at 21 Hz and 41 Hz, respectively. PAC between theta phase and gamma power was spatially specific, only occurring when response fields overlapped the cued location. When response fields instead overlapped the uncued location, there were two significant peaks in PAC between theta phase and beta power, at 16 Hz and 30 Hz (permutation test, $p < 0.001$).

In addition to temporally coordinating within-region neural activity (Fig. 4A, B), PAC represents a potential mechanism for synchronizing higher-frequency activity across anatomically distant brain regions, thereby facilitating between-region communication (Canolty and Knight, 2010). Figure 4 (C, D) shows significant PAC between theta phase in FEF (at 4–6 Hz) and both alpha (at 9–16 Hz) and beta (at 23–31 Hz) power in LIP (permutation test, $p < 0.001$), with peaks at 12 Hz and 27 Hz, respectively. As with the within-region results (in FEF), PAC between theta phase in FEF and beta power in LIP was not spatially specific, occurring regardless of whether response fields overlapped either the cued location or the uncued location. That is, theta phase in FEF was linked to beta power in FEF and LIP, both inside and outside the primary focus of spatial attention. In contrast, PAC between theta phase in FEF and alpha power in LIP was spatially specific, exclusively occurring when response fields overlapped the cued location (i.e., inside the primary focus of spatial attention).

There was also significant PAC between theta phase in LIP (at 4–6 Hz) and gamma power in FEF (at 32–44 Hz), with a peak at 38 Hz (permutation test, $p < 0.001$). This effect was significantly greater when response fields overlapped the cued location relative to when response fields overlapped the uncued location (at 33–45 Hz). As with the within-region results (in LIP), PAC between theta phase in LIP and gamma power in FEF was spatially specific, only occurring when response fields overlapped the cued location (Fig. 4C, D). That is, theta phase in LIP was linked to gamma power in both FEF and LIP, but only under conditions of spatial attention.

To summarize our PAC results, theta phase measured in LIP was most strongly associated with gamma power (both locally and within FEF), while theta phase measured in FEF was most strongly associated with beta power (both locally and within LIP). Peaks in PAC between theta phase and higher-frequency power generally overlapped with the previously described, theta-dependent links between oscillatory phase and behavioral performance (Fig.

3E, F). For both of these analyses (Figs. 3, 4), beta-band/gamma-band activity and alpha-band activity were linked to opposite theta phases. Increased beta and gamma power seem to be associated with the “good” theta phase, while increased alpha power seems to be associated with the “poor” theta phase.

Because differences in power between conditions can lead to spurious differences in PAC (Aru et al., 2015), we performed a control analysis, equating both theta power and higher-frequency power across conditions (see STAR Methods; Fig. S9). The results of this control analysis confirmed the between-condition differences shown in Figure 4 (B, D). We additionally performed a control analysis to test whether theta-dependent changes in oscillatory power were associated with the occurrence of microsaccades. These small, fixational eye movements have previously been linked to theta-band activity in visual cortex (Bosman et al., 2009) and changes in visual processing in FEF (Chen et al., 2015). Here, we used a subset of recording sessions where eye position was sampled at a high enough rate (1000 Hz) to detect microsaccades (see STAR Methods). Our results show that PAC between theta phase and higher-frequency power remained statistically significant after the removal of trials with microsaccades during the cue-target delay (Fig. S10). These findings are in agreement with other studies that have similarly shown that behavioral and neural effects associated with theta-rhythmic sampling cannot be explained by the occurrence or rate of microsaccades (Landau et al., 2015; Spyropoulos et al., 2018).

Theta rhythms play a key role in coordinating neural activity in the frontoparietal network (Fig. 4), with interactions between theta phase and higher-frequency power shaping environmental sampling (and sampling rates). Below we describe the functional significance of theta-dependent changes in alpha, beta, and gamma power, within the context of our broader model for the neural basis of rhythmic sampling (see the Discussion).

Two theta-dependent attentional states

We have thus far demonstrated that oscillatory phase in the frontoparietal network is coupled to both behavioral performance (i.e., HRs) and oscillatory power (i.e., through PAC). It follows that behavioral performance and oscillatory power should also be correlated with each other. Figure S11 (A, B) confirms this prediction, demonstrating significant power-detection relationships (permutation test, $p < 0.0009$). Higher theta and beta power in FEF and higher gamma power in LIP are predictive of better behavioral performance at the cued location. Moreover, measuring these power-detection relationships at different time points relative to target presentation (Fig. S11C–H) provides further evidence of an ongoing, rhythmic process associated with environmental sampling (see STAR Methods). Underlying these rhythmic properties of spatial attention, neural activity in the frontoparietal network seems to alternate between two states, characterized by (i) different temporal dynamics and (ii) better or worse behavioral performance. Specifically, periods of higher beta/gamma power (in FEF and LIP) and higher detection rates are interdigitated with periods of higher alpha power (in LIP) and lower detection rates (Figs. 3, 4).

We next tested whether theta-band activity, which seems to coordinate these alternating attentional states, is synchronized across the frontoparietal network. Figure 5 (A) demonstrates such synchronization, showing statistically significant theta peaks (at 5 Hz and

7 Hz) for LFP-LFP phase coupling between FEF and LIP when response fields overlapped the cued location (permutation test, $p < 0.001$). Between-condition comparisons further revealed significantly stronger LFP-LFP phase coupling in the theta band when response fields overlapped the cued location relative to when response fields overlapped the uncued location (permutation test, $p < 0.008$). To further probe theta-band coupling between FEF and LIP, we also measured between-region, spike-LFP phase coupling. This measure of between-region synchronization examines the clustering of spikes around oscillatory phases in the LFP signal. Unlike LFP-LFP phase coupling, spike-LFP phase coupling is not influenced by synchronization resulting from a common recording reference. Rather than combining all neurons, we calculated spike-LFP phase coupling within specific cell classes (i.e., visual and visual-movement neurons), helping to elucidate the functional role of between-region synchronization. Our goal was to establish whether spikes in FEF and/or LIP were correlated with theta phase (in the LFP signal). Figure 5 (B) shows between-region spike-LFP phase coupling when receptive/response fields overlapped either the cued or the uncued location. The data revealed significant coupling between spikes in FEF and theta phase in LIP when receptive/response fields overlapped the cued location (permutation test, $p < 0.001$), as well as a statistically significant difference between the two conditions (i.e., cued vs. uncued; permutation test, $p < 0.008$). These effects were exclusively observed in the population of visual neurons (see Fig. 6 for spike-LFP phase coupling by functionally defined cell classes).

When measuring between-region spike-LFP phase coupling, spikes are typically viewed at reflecting regional output, while LFPs are viewed as reflecting regional input (Pesaran, 2010). The present findings therefore provide evidence that spatial attention is associated with theta-band activity in FEF, which propagates to LIP. Granger causality, which measures the influence that one area (e.g., FEF) has on another area (e.g., LIP), supports the same conclusion (Fig. 5C). Under conditions of spatial attention, the FEF influence on theta-band activity in LIP was significantly greater than the LIP influence on theta-band activity in FEF (permutation test, $p < 0.008$). These findings thus indicate that theta phase in FEF organizes rhythmic sampling during spatial attention, providing the clocking mechanism that coordinates two rhythmically alternating attentional states. Figure S12 shows comparable results for theta-band synchronization after equating theta power between conditions (i.e., cued vs. uncued) and/or brain regions (i.e., FEF and LIP).

Spike-LFP phase coupling at higher frequencies

We also measured spike-LFP phase coupling outside the theta band, investigating between-region synchronization at the higher frequencies that define theta-dependent attentional states: alpha, beta, and gamma. Figure 6 shows spike-LFP phase coupling by functionally defined cell classes, from 3–60 Hz. These results provide further detail regarding interactions between FEF and LIP. First, beta-band synchronization during spatial attention was exclusively observed in visual-movement neurons (i.e., neurons with both saccade-related activity and visual-sensory responses). Second, gamma-band synchronization was exclusively observed between spikes in LIP and LFPs in FEF (and not in the opposite direction), suggesting that gamma-band activity originates in LIP and propagates to FEF. To clarify, although there was no significant difference in gamma-band synchronization

between the cued and uncued conditions (Fig. 6B), spike-field phase coupling in the gamma band was statistically significant when receptive fields and response fields overlapped the cued location (Fig 6D). These findings help to frame our interpretation of the results (see the Discussion section).

Unlike the beta and gamma bands, we found no evidence of between-region spike-LFP phase coupling in the alpha band. The present analyses are focused on FEF and LIP, but we also recorded from the pulvinar nucleus of the thalamus, specifically the mediodorsal subdivision that is interconnected with the frontoparietal network (Saalmann and Kastner, 2011). Our data indicate that alpha-band activity in LIP is closely associated with this third region of interest, but we will present those findings elsewhere.

DISCUSSION

The present results provide the first evidence of rhythmic sampling during spatial attention in monkeys (Fig. 2), mirroring behavioral evidence in humans (Fiebelkorn et al., 2013a; Helfrich et al., 2018). These findings thus suggest that rhythmic sampling is a fundamental property of spatial attention, having been evolutionarily preserved across at least two primate species. After establishing rhythmic properties of spatial attention at the behavioral level, we investigated the neural basis of this rhythmic sampling, emphasizing links between behavioral performance (i.e., HRs) and neural oscillatory activity in FEF and LIP. Our data demonstrate that neural oscillations in the frontoparietal network have critical consequences for sensory processing (Fig. 3). That is, our data are consistent with neural oscillations in FEF and LIP shaping behavioral performance during spatial attention. We observed significant relationships between oscillatory phase and visual-target detection across multiple frequency bands, but our data converge on a single, theta-dependent sampling process (Figs. 3, 4).

Theta rhythms are prominent in both rodents and primates and have been linked to multiple brain regions, most frequently to the medial temporal lobe and prefrontal cortex (Colgin, 2013). The functional role of theta rhythms in these brain regions is typically discussed in the context of either memory (Liebe et al., 2012; Lisman and Jensen, 2013; Siegel et al., 2009) or environmental navigation (Killian et al., 2012; Moser et al., 2008). Theta rhythms, however, also play a key role in environmental sampling, whether through covert (Busch and VanRullen, 2010; Dugue et al., 2016; Fiebelkorn et al., 2013a; Landau and Fries, 2012; Landau et al., 2015; VanRullen et al., 2007) or overt (Berg and Kleinfeld, 2003; Bosman et al., 2009; Fanselow and Nicolelis, 1999; Hogendoorn, 2016; Otero-Millan et al., 2008; Wutz et al., 2016) mechanisms. Previous studies investigating the neural basis of theta-rhythmic sampling in primates have focused on visual cortex (Bosman et al., 2009; Landau et al., 2015). However, studies in rodents suggest stronger correlations between theta-band activity (in somatosensory cortex) and environmental sampling during goal-directed behavior (Ganguly and Kleinfeld, 2004), thus implicating the involvement of higher-order brain regions. Here, we investigated links between theta-rhythmic sampling and the frontoparietal network that directs spatial attention and eye movements (Bisley and Goldberg, 2010; Buschman and Miller, 2007; Corbetta et al., 1998; Squire et al., 2013). Our results indicate that theta-band activity provides a clocking mechanism that temporally coordinates two

alternating states. The first theta-dependent state, associated with better behavioral performance, appears to be characterized by both FEF-dominated beta-band activity (Figs. 4, S11) and LIP-dominated gamma-band activity (Figs. 4, 6, S11). The second theta-dependent state, associated with worse behavioral performance, appears to be characterized by LIP-specific alpha-band activity (Figs. 4, 6).

The present data suggest that theta-band activity during spatial attention originates in FEF and propagates to LIP (see also Sellers et al. (2016)). We propose that theta-band activity from FEF similarly propagates to visual cortex, leading to theta-rhythmic fluctuations in gamma power (Landau et al., 2015; Spyropoulos et al., 2018). As with the present study, previously described theta-dependent increases in gamma-band activity in human visual cortex have been linked to better behavioral performance (i.e., higher hit rates) (Landau et al., 2015). We therefore speculate that the “good” theta phase (Fig. 3A, B) is associated with temporally aligned increases in gamma power across FEF, LIP, and visual cortex. It should be noted, however, that Esghaei et al. (2015), who recorded from visual cortex (i.e., area MT) in macaques, described a decrease in PAC between the phase of low-frequency oscillations (1–8 Hz) and gamma power (30–120 Hz) during spatial attention (see also Spyropoulos et al., 2018). This attention-related decrease in PAC contrasts with the present findings, which describe an increase in PAC during spatial attention (Fig. 4). Previous studies recording from frontal and parietal cortices have similarly described an attention-related increase in PAC between theta phase and gamma power (Sellers et al., 2016; Szczepanski et al., 2014). The reasons for this apparent discrepancy between recordings in visual cortex and the frontoparietal network are yet unknown. At least one study, investigating short-term memory, has demonstrated theta-band synchronization between frontal and visual cortices (Liebe et al., 2012). Future studies will need to establish whether such theta-band synchronization (between visual cortex and the frontoparietal network) is similarly utilized during spatial attention, perhaps organizing incoming sensory information into discrete samples.

Considerable evidence from previously published studies indicates that the spatially specific increase in gamma-band activity—observed during the “good” theta phase—is associated with enhanced visual processing at the cued location. That is, neurons in visual cortex show increased gamma synchronization when their receptive fields overlap an attended stimulus relative to when their receptive fields overlap an unattended stimulus (Bichot et al., 2005; Fries et al., 2001), with consequences for behavioral performance (Womelsdorf et al., 2006). Gamma-band activity in visual cortex is also linked to between-region synchronization during spatial attention (Bastos et al., 2015; Bosman et al., 2012; van Kerkoerle et al., 2014), potentially facilitating interregional communication (Fries, 2015). These findings extend into the frontoparietal network (Gregoriou et al., 2009), where Buschman and Miller (2007) reported attention-related gamma-band synchronization between FEF and LIP. Similar to their results, the present findings suggest that gamma-band activity is more closely associated with LIP (Figs 2–4, S11), perhaps originating there and propagating to FEF (Fig. 6). We further demonstrate that attention-related gamma-band activity is modulated by theta phase (Figs. 3, 4), leading to periodic (rather than continuous) boosts in visual processing at the cued location (i.e., rhythmic sampling).

In addition to theta-dependent increases in gamma-band activity when response fields overlapped the cued location, the present results revealed co-occurring, theta-dependent increases in beta-band activity. These increases in beta-band activity occurred regardless of whether response fields overlapped the cued or the uncued location. Previous studies have linked beta-band activity with top-down (or feedback) deployments of spatial attention (Bastos et al., 2015), suggesting sources in frontal cortex (Buschman and Miller, 2007, 2009). In the present study, specificity in spike-LFP phase coupling provided further clues regarding the functional significance of beta-band activity. That is, beta-band synchronization exclusively occurred in neurons with saccade-related responses (i.e., the population of visual-movement neurons; Fig. 6). Gregoriou et al. (2012) reported a similar link, in FEF, between beta-band synchronization and neurons with saccade-related responses, interpreting their results in the context of sensorimotor suppression. Beta-band activity typically increases during periods of motor inactivity and decreases during periods of motor preparation or execution (Pogosyan et al., 2009; Zhang et al., 2008). Here, we report spatially non-specific, theta-dependent increases in beta-band activity, which are associated with better behavioral performance at the cued location. We propose that these rhythmic fluctuations in beta-band activity reflect the pulsed suppression of attentional shifts (and/or eye movements). That is, during periods of increased beta-band activity (i.e., during the “good” theta phase), there is a decreased likelihood of attentional shifts away from the cued location, contributing to better behavioral performance. During periods of decreased beta-band activity (i.e., during the “poor” theta phase), there is an increased likelihood of attentional shifts, contributing to worse behavioral performance at the cued location (and perhaps better behavioral performance elsewhere in the visual field (Fiebelkorn et al., 2013a)).

In addition to decreased beta-band activity (and decreased gamma-band activity), the “poor” theta phase is associated with an increase in LIP-specific alpha-band activity (Fig. 3, 4). Much of the research on oscillatory processes in the human brain has focused on the alpha band. This literature reveals a strong correlation between alpha power and the suppression of cortical processing. For example, alpha power increases over parieto-occipital cortex contralateral to a to-be-ignored (i.e., uncued) visual hemifield (Worden et al., 2000), reflecting an active suppression of visual processing in that hemifield (Kelly et al., 2006). While there have been far fewer neurophysiological studies in non-human primates investigating the functional role of alpha rhythms, the studies that do exist have largely drawn the same conclusions (Bollimunta et al., 2008; Bollimunta et al., 2011; Buffalo et al., 2011; Haegens et al., 2011). Haegens et al. (2011) recorded from sensorimotor regions (i.e., somatosensory, premotor, and motor cortex) while a monkey performed a vibrotactile discrimination task. Higher alpha-band activity during the discrimination task was associated with both lower spike rates and worse behavioral performance.

The present results similarly link increases in alpha-band activity with worse behavioral performance (Figs. 3, 4). We propose that increased alpha power during the “poor” theta phase reflects an attenuation (or suppression) of visual processing at the cued location. This attenuation provides windows of opportunity when behaviorally relevant stimuli outside the focus of spatial attention can more easily prompt an attentional shift. Environmental sampling is guided by a priority map, which is largely informed by stimulus salience and

behavioral goals (Fecteau and Munoz, 2006). By periodically attenuating the strongest peak in that priority map, the rhythmic properties of spatial attention promote active sampling (Schroeder et al., 2010), preventing spatial attention from remaining overly focused on a single location. If an attentional shift does occur during the “poor” theta phase, we speculate that this alpha-driven attenuation at the previously attended location might persist, contributing to the inhibition of return phenomenon (Posner et al., 1985). Inhibition of return refers to the temporary suppression of a location (or stimulus) that was previously the focus of attention.

Whereas other intracortical studies linking behavioral performance to alpha-band activity have largely focused on sensory cortices (Bollimunta et al., 2008; Bollimunta et al., 2011; Haegens et al., 2011), here we link behavioral performance to alpha-band activity in higher-order cortex, specifically a region involved in directing spatial attention (Bisley and Goldberg, 2010). Human EEG/MEG studies investigating the role of alpha oscillations in spatial attention have frequently localized their effects to parieto-occipital cortex (Kelly et al., 2006). Parietal regions (e.g., LIP in monkeys) might serve as a cortical generator of alpha oscillations, which then spread to visual-cortical (i.e., occipital) regions to suppress processing of to-be-ignored locations.

The “poor” theta phase is associated with diminished visual-target detection relative to the “good” theta phase. However, it remains unclear how visual-target detection during the “poor” theta phase compares between the cued and uncued locations. That is, the present results cannot distinguish among three possibilities: (i) visual-target detection remains somewhat elevated at the cued location relative to the uncued location, (ii) visual-target detection is equivalent between the two locations, and (iii) visual-target detection is somewhat attenuated at the cued location relative to the uncued location. Future studies will need to further investigate such relative differences in behavioral performance.

Figure 7 presents our biphasic model of spatial attention, which summarizes the present findings. Here, we link rhythmic sampling during spatial attention to nested oscillatory activity in the frontoparietal network. Theta phase governs rhythmically alternating attentional states, defined by either (i) FEF-dominated beta-band activity and LIP-dominated gamma-band activity, or (ii) LIP-specific alpha-band activity. We propose that the first attentional state reflects suppressed attentional shifts away from the cued location and enhanced visual processing at the cued location, while the second attentional state reflects an attenuation of visual processing at the cued location, perhaps in preparation for a potential attentional shift (Benedetto and Morrone, 2017). These alternating attentional states lead to rhythmic sampling of the visual environment and thus rhythmic fluctuations in perceptual sensitivity (as measured in behavioral performance).

Our model of spatial attention assigns functions to theta-dependent attentional states based, in part, on previously established associations with specific oscillatory frequencies (e.g., increased alpha-band activity has been repeatedly linked to the attenuation of sensory processing). We do not intend to imply, however, that temporal dynamics (e.g., oscillatory frequencies) determine function. Attention-related temporal dynamics emerge from properties of the underlying neural circuitry. That is, the properties and connectivity patterns

of neurons determine both temporal dynamics and function. For example, Kienitz et al. (2018) recently provided evidence that theta-band oscillations in visual cortex (i.e., V4) arise from receptive field interactions, specifically occurring when separate visual stimuli are presented in the excitatory center and suppressive surround of neuronal receptive fields (see also Rollenhagen and Olson, 2005). Moldakarimov et al. (2005) suggested that such low-frequency oscillatory activity in response to multiple visual stimuli could rely on a couple of parameters: (i) the strength of inhibition between competing neuronal pools and (ii) neuronal fatigue. Future studies (e.g., using multi-contact recording arrays and/or causal manipulations) will need to further parse the specific neural circuitry underlying rhythmic spatial attention.

In addition to electrophysiological recordings in monkeys, we have investigated the neural basis of theta-rhythmic sampling using large-scale, subdural recordings in pharmacoresistant epilepsy patients (Helfrich et al., 2018). Electrocorticography (ECoG) provides variable but more extensive cortical coverage, yet our results similarly link theta-rhythmic sampling during spatial attention to theta-band activity in the frontoparietal network. In the ECoG study, we specifically show that theta phase is correlated with changes in cortical excitability (as measured through theta-dependent changes in high-gamma power). We further demonstrate that our ECoG findings are consistent across two different behavioral tasks, providing evidence that theta-rhythmic sampling is not task driven, but rather an intrinsic property of spatial attention. One of those behavioral tasks is the same variant of the Egly-Driver task (Fig. 1) that we used during monkey recordings, thereby providing complementary results in two primate species.

Theta-band rhythms are broadly characteristic of environmental sampling, having now been linked to covert spatial attention (Busch and VanRullen, 2010; Fiebelkorn et al., 2013a; Landau and Fries, 2012; Landau et al., 2015; VanRullen et al., 2007) and eye movements in primates (Bosman et al., 2009; Hogendoorn, 2016; Otero-Millan et al., 2008; Wutz et al., 2016) and whisking in rodents (Berg and Kleinfeld, 2003; Fanselow and Nicolelis, 1999). In primates, the frontoparietal network has an established role in mediating both spatial attention and eye movements (Corbetta et al., 1998). Theta rhythms might therefore serve to temporally resolve functional conflicts in this network, organizing neural activity into alternating attentional states that promote either sampling (i.e., during the “good” theta phase) at the present target location or shifting to another target location (i.e., during the “poor” theta phase).

STAR METHODS

CONTACT FOR REAGENT AND RESOURCE SHARING

Further information and requests for resources and reagents should be directed to and will be fulfilled by the lead contact, Ian Fiebelkorn (iancf@princeton.edu).

EXPERIMENTAL MODEL AND SUBJECT DETAILS

The study used two male *Macaca fascicularis* monkeys (6–9 years old). The Princeton University Animal Care and Use Committee approved all procedures, which conformed to

the National Institutes of Health guidelines for the humane care and use of laboratory animals.

METHOD DETAILS

Behavioral Task—We trained the monkeys to perform a variant of the Egly-Driver task (Egly et al., 1994), using Presentation software to control stimuli, monitor responses, and trigger reward delivery. An auditory "go" tone indicated the beginning of each trial. The monkeys initiated the trial sequence by depressing and holding down a lever. At trial onset, a fixation square (0.5°) appeared at the center of the monitor (eye-monitor distance = 57 cm). After a variable delay of 500–1200 ms, two-bar shaped objects (22° × 4.4°) appeared. These bars were presented either to the left and right of central fixation (vertically oriented) or above and below central fixation (horizontally oriented), with equal probability. The closest edge of each bar was 6.6° from central fixation. After a second variable delay of 500–1200 ms, a spatial cue briefly appeared (100 ms), surrounding the end of one of the bar-shaped objects (Fig. 1A, B). This cue indicated where a subsequent visual target was most likely to occur (with 78% cue validity). After a third variable delay (i.e., the cue-target delay) of 300–1600 ms, a low-contrast (2.5–4%) target briefly appeared (100 ms) at the end of one of the bar-shaped objects. The closest corner of the target (4.4° × 4.4°) was 9.4° from central fixation. If the target was not presented at the cued location, it could instead appear at one of the two equidistant, uncued locations (12% of all trials), split evenly between the uncued location on the same object as the cued location (i.e., the same-object location) and the uncued location on the second object (i.e., the different-object location). For the present manuscript, all of our analyses are focused on either the cued location (i.e., the attended condition; Fig. 1A) or the different-object location (i.e., our baseline condition; Fig. 1B). The monkeys released the lever when they detected a target, receiving a juice reward for correct responses (150 to 650 ms after the target). Behavioral data are reported in Table S1. On 10% of trials, no visual target occurred following the spatial cue (i.e., catch trials). The monkeys instead released the lever when the screen cleared, 1600 ms after the cue. We monitored eye position using an infrared eye tracker (either an Eye-trac 6 at 240 Hz from Applied Science Laboratories or an EyeLink 1000 Plus at 1000 Hz from SR Research), and trials were aborted if eye position deviated by more than one degree from central fixation (i.e., if the monkey broke fixation). Visual stimuli appeared on a 21-inch CRT monitor set at a refresh rate of 100 Hz, and we verified stimulus timing using a customized photodiode system.

Electrophysiology—All surgical procedures were performed under general anesthesia with isoflurane (induction 2– 5%, maintenance 0.5– 2.5%) and under strictly aseptic conditions. We used titanium skull screws and bone cement to affix head implants and two customized plastic recording chambers (one frontal and one parietal) to the animals. After recordings in the left hemisphere, the chambers were moved to the right hemisphere for additional recordings. Craniotomies (4.5 mm diameter) provided access to our regions of interest (ROIs). We fitted each craniotomy with a conical plastic-guide tube filled with bone wax (Pigarev et al., 2009). These wax-filled guide tubes held glass-coated platinum-iridium electrodes (impedance: 5 MΩ) in place between recording sessions. Each recording session spanned a few hours, with up to seven sessions per week.

During recordings, we stabilized the animal's head using four thin rods that slid into hollows in the side of the implants. We independently lowered electrodes with microdrives (NAN Instruments) coupled to an adapter system that allowed different approach angles for each ROI. Electrode signals (40,000 Hz sample rate for spikes; 1,000 Hz sample rate for LFPs) were amplified and filtered (150–8,000 Hz for spikes; 0.7–300 Hz for LFPs) using a Plexon preamplifier with a high input impedance headstage and Multichannel Acquisition Processor (MAP) controlled by RASPUTIN software.

Prior to experimental recordings, we simultaneously recorded neural signals from three skull screws, one in each chamber and one placed over the opposite hemisphere (i.e., outside the chambers). We alternated across control recording sessions, using each skull screw as the reference electrode. After verifying the absence of visual and attention-related responses, we selected the skull screw placed over the opposite hemisphere as the reference electrode for all experimental recording sessions.

During recordings, we sorted spikes online to isolate neurons, then we re-sorted spikes for offline analyses using Plexon Offline Sorter software. The Egly-Driver task has four target locations, one in each quadrant. We used a quadrant-mapping task (i.e., large Gabor stimuli flashed in each quadrant), the spatial cue, and the target to determine the quadrant where individual neurons and LFPs had their strongest responses. Figure S8 shows quadrant-specific responses from two typical recording sessions in FEF. Figure S13 shows population PSTHs for both FEF and LIP, with each neuron's spiking activity first sorted by the strength of its response to cues (0–250 ms post cue) presented in each quadrant (i.e., responses were sorted strongest to weakest). There was typically a strong bias toward stimuli in a single quadrant, with relatively weak responses when stimuli occurred elsewhere (Figs. S8, S13).

Here, we present data from 97 recording sessions in FEF (monkey L: N = 58, monkey R, N = 39) and 98 recording sessions in LIP (monkey L: N = 45, monkey R: N = 53). We also simultaneously recorded from the medial pulvinar nucleus of the thalamus, but those data will be reported elsewhere. There were 67 recording sessions (monkey L: N = 39, monkey R: N = 29) when FEF and LIP had their strongest responses to stimuli within the same visual quadrant (i.e., aligned RFs and/or multi-unit RFs). We used these recording sessions for between-region analyses. Across all recording sessions, we isolated 98 neurons in FEF and 98 neurons in LIP that had significantly increased spike rates in response to the cue (FEF: N = 36, LIP: N = 39), the target (FEF: N= 17, LIP: N = 18), or both the cue and the target (FEF: N= 45, LIP: N = 41). These counts only include neurons with their strongest responses to stimuli in the contralateral hemifield. There was an additional, small population of neurons that demonstrated either significantly decreased spike rates or their strongest responses to stimuli in the ipsilateral hemifield (FEF: N = 16, LIP: N = 7).

Acquisition of Structural Images for Electrode Positioning—The animals were sedated with ketamine (1-10mg/kg i.m.) and xylazine (1-2 mg/kg i.m.), and provided with atropine (0.04 mg/kg i.m.). Sedation was maintained with tiletamine/zolazepam (1-5mg/kg i.m.). We then placed the animals in an MR-compatible stereotaxic frame (1530M; David Kopf Instruments, Tujunga CA) and monitored vital signs with wireless ECG and respiration sensors (Siemens AG, Berlin), and a fiber optic temperature probe (FOTS100; Biopac

Systems Inc, Goleta CA). Body temperature was maintained with blankets and a warm water re-circulating pump (TP600; Stryker Corp, Kalamazoo MI).

We collected structural MRI data for the whole brain on a Siemens 3T MAGNETOM Skyra using a Siemens 11-cm loop coil placed above the head. T2-weighted images were acquired with a 3-dimensional turbo spin echo with variable flip-angle echo trains (3D T2-SPACE) sequence (voxel size: 0.5mm, slice orientation: sagittal, slice thickness: 0.5mm, field of view (FoV): 128mm, FoV phase: 79.7%, repetition time (TR): 3390ms, echo time (TE): 386ms, base resolution: 256, acquisition time (TA): 17min 51sec). We used these images both to select coordinates for chamber placements and to position electrodes for recordings. Platinum-iridium electrodes create a clearly identifiable, susceptibility-induced signal void along the length of the electrodes in structural MRI images. This “shadow” has a width of approximately one voxel (0.5 mm^3 on either side of the electrode), allowing us to visualize electrode placement (Fig. S1).

Prior to recordings, we positioned electrodes just dorsal to our ROIs. The electrodes were then held *in situ* by customized guide tubes and lowered into cortex over the course of typically one week of recordings. We then acquired additional structural MRI data prior to replacing the electrodes. We used the before and after images, as well as daily microdrive measurements, to reconstruct electrode tracks.

To further localize electrode penetrations, we aligned the D99 digital template atlas to each individual animal’s MRI volume, using a combination of FSL and AFNI software tools (Cox, 1996; Jenkinson et al., 2012; Reveley et al., 2017). The D99 atlas is based on and aligned to MRI and histological data from the Saleem and Logothetis (2007) atlas, and allows identification of labeled areas within the native 3D MRI volume of an individual animal. Briefly, we first extracted the brains from the MRI volumes using the FSL brain extraction tool (BET) (Smith, 2002). Next, to improve alignment accuracy, we inverted the contrast of the MRI volumes to resemble the image contrast of the T1-weighted atlas MRI volume. We then implemented the pipeline provided by Reveley et al. (2017) to align the atlas to each monkey’s MRI volume. This pipeline included a sequence of affine and nonlinear registration steps to first align the individual animal’s MRI volume to the atlas, then inverting the transformations to warp the atlas to the animal’s original native space. Once aligned, we visually overlaid the atlas’ anatomical subdivisions upon the individual monkey’s MRI volume to assist in the electrode localizations.

For all recordings presented here, the electrodes were positioned in atlas-defined FEF and LIP. Figure S1 provides examples of localizations from two representative penetrations. According to the histological atlas (Saleem and Logothetis, 2007), area FEF (8A) spans +25 to +35 and area LIP spans −6 to +7 in the anterior-posterior (AP) direction. When the atlas is warped to the anatomy of animal R, area FEF instead spans +23 to +27 and area LIP instead spans −5.5 to +9 in the AP direction. Similarly, when the atlas is warped to animal L’s anatomy, area FEF instead spans +23.5 to +28 and area LIP instead spans −7.5 to +8 in the AP direction. All recording sites in each animal were located within the areas defined by the warped atlas, as Figure S1 illustrates.

QUANTIFICATION AND STATISTICAL ANALYSIS

Data from the two animals were qualitatively similar, so we combined them for all analyses. Both monkeys demonstrated significantly better visual-target detection at the cued location (Table S1), significantly increased spiking activity during the cue-target delay, significant theta-band rhythmicity in their behavioral data, and statistically significant phase-amplitude coupling (Fig. S14).

Spike Rate—For all analyses, we used a combination of customized Matlab functions and the Fieldtrip toolbox (Oostenveld et al., 2011) (http://www.ru.nl/neuroimaging/fieldtrip). To estimate changes in spike rate over time, time-locked to either the cue or the target, we convolved spikes from each trial with a Gaussian filter (σ = 10 ms) and averaged the resulting functions. For each neuron, we determined whether there was a statistically significant increase in spike rate in response to the cue or the target (i.e., within 250 ms after cue or target presentation) by using a non-parametric randomization procedure. We randomly selected one response value from the pre-cue period (−350–0 ms) of each trial, averaging those values across trials. We repeated this procedure 5000 times to generate a reference distribution (for the baseline spike rate). The p-value for a non-parametric test is the proportion of values in the reference distribution that exceeds the test statistic (i.e., the observed value from collected data). For all statistical comparisons, unless otherwise specified, we adopted an alpha criterion of 0.05, and used the Holm's sequential Bonferroni correction to control for multiple comparisons.

To create population PSTHs, we normalized the spike rate for each neuron by its maximum response during trials, and then grand-averaged the normalized rates across neurons. To test whether between-condition comparisons (i.e., cued vs. uncued) were statistically significant (i.e., to establish significant attention effects), we used a Wilcoxon rank-sum test, after averaging the response in a 500-ms window preceding the target (Fig. S4).

LFP Power Estimates (i.e., Spectograms)—To examine frequency-specific changes in LFP power, time-locked to the target, we first bandpass filtered the LFPs across multiple frequency bands, using 5-Hz windows and 2-Hz steps from 3–56 Hz (e.g., 3–8, 5–10, 7–12...). We then used the Hilbert transform to generate the analytic signal. Using this complex output, we derived power estimates relative to a pre-cue baseline (from −250 to −50 ms prior to the cue). Specifically, we calculated the percent change in power from the pre-cue baseline by (1) subtracting the frequency-specific, averaged baseline power from each time point, (2) dividing by the averaged baseline power, and (3) multiplying by 100. We then averaged data across recording sessions, separately for FEF and LIP. To avoid overlap with the cue response (i.e., the initial sensory response), we only used trials that had a cue-target delay of at least 950 ms (also used for all subsequent analyses). Figure S5 illustrates the difference in oscillatory power when response fields encompassed the cued location relative to when response fields encompassed the uncued location. We were specifically interested in oscillatory activity associated with rhythmic sampling. We therefore did not consider frequencies above 60 Hz, which have been shown to reflect a broadband, non-oscillatory phenomenon (Manning et al., 2009; Miller et al., 2007). To test whether target-locked changes in oscillatory power were significantly different across conditions (i.e., cued vs.

uncued), we used a Wilcoxon rank-sum test (accounting for multiple comparisons), after first averaging the frequency-specific responses over a 500-ms window preceding the target.

Oscillations in Behavioral Data—The approach we used in the present experiment is identical to that detailed in a previous study that measured oscillations in human behavioral data (Fiebelkorn et al., 2013a). That study used a nearly identical variant of the Egly-Driver task to manipulate attentional deployment. Here, behavioral data from two monkeys were compiled across recording sessions (N = 130) with a hit rate (HR) of less than 85% at the cued location (to avoid ceiling effects). We measured HRs as a function of the cue-target interval, binning trials within a sliding, 50-ms window. Figure S2 shows how the results vary using different window lengths (i.e., 30-ms, 40-ms, or 50-ms) to bin the data. We then used the spectral amplitudes from a fast Fourier transform (FFT) of the behavioral time-series data to establish whether linearly detrended HRs following the spatial cue demonstrated an oscillatory component (from 3–12 Hz). We established statistical significance by (i) reshuffling hits and misses across cue-target delays (5000 times) and then (ii) repeating our analysis steps to generate a reference distribution. P-values were based on the number of values in the reference distributions that were exceeded by the observed spectral amplitude, separately for each frequency (controlling for multiple comparisons).

The preferable metric for measuring perceptual sensitivity is d', which takes into account both HRs and false alarm rates. For a couple of reasons, however, it was not possible to accurately estimate d' in the present experiment. First, the monkeys had a single response (i.e., releasing the lever), regardless of the location where they saw (or believed they saw) a visual target. That means it is impossible to assign false alarms to a specific condition (cued vs. uncued). It is also impossible to know exactly when the monkeys thought they saw the target during false-alarm trials, which would be critical for tracking temporal fluctuations in d'. That is, to estimate d' at different cue-target delays, we would need to be able to assign false alarms to different time bins.

Importantly, false alarm rates were not high for either animal (approximately 10% for each of the two animals across all sessions; Table S1), meaning that d' estimates would be largely determined by HRs. As an additional control analysis, we re-ran our behavioral analyses after excluding sessions with greater than a 10% false alarm rate. The average false alarm rate among the remaining sessions was 5%. Removing sessions with a higher false alarm rate did not substantially alter our results. That is, we still observed significant theta-band rhythmicity in visual-target detection.

Intertrial Phase Consistency—Several studies in humans have shown that the phase of neural oscillatory activity is correlated with behavioral performance (VanRullen, 2016). Rhythmicity in behavioral data, which is visualized by binning data across trials based on their cue-target delays, seemingly necessitates a consistent phase reset of neural oscillatory activity. That is, rhythmicity in behavioral data suggests a consistent relationship between behavioral performance and the length of the cue-target delay. This relationship might be established by a phase-resetting event (e.g., a spatial cue) that aligns the phase of neural oscillatory activity across trials. We therefore used intertrial phase consistency (Makeig et al., 2002) to test for cue-locked phase alignment in FEF and LIP.

We first convolved complex Morlet wavelets with the cue-locked LFP signal (−700 to 950 ms), from 3 to 60 Hz (in 1-Hz steps), only using trials when the bars and the target occurred at least 950 ms before and after the cue, respectively. The width of these wavelets was two to five cycles (3–10 Hz = 2 cycles; 11–14 Hz = 3 cycles; 15–20 Hz = 4 cycles; > 20 Hz = 5 cycles). We then normalized the complex result of the wavelet convolution by its amplitude, separately for each frequency and time point. Finally, we averaged the normalized complex vectors and took the absolute value of that average (Fig. S3). ITPC values range from zero (no phase locking) to one (perfect phase locking).

To test for statistical significance, we compiled frequency-specific reference distributions by randomly selecting complex values (normalized by their amplitudes) from a precue baseline period (−450 to −250 ms), avoiding contamination from visual-sensory responses to either the bar or the cue. We then computed ITPC based on these randomly selected complex values from each trial, repeating this procedure 1500 times. We established statistical significance by comparing our observed ITPC values with these reference distributions (controlling for multiple comparisons).

Phase-Detection Relationships—For this analysis, our goal was to test whether oscillatory phase in the frontoparietal attention network was linked to behavioral performance during spatial attention. We adapted an approach previously applied to EEG data (Fiebelkorn et al., 2013b). We first convolved complex Morlet wavelets with the LFP signal just prior to target presentation. We then took the angle of the complex output, deriving pre-target phase estimates, aligned such that the temporal extent of the wavelet did not overlap with the target response. For all spectral analyses, we focused on the cue-target delay (i.e., under conditions of covert, sustained spatial attention), which generally satisfied methodological assumptions of stationarity (Jarvis and Mitra, 2001).

We next sorted trials by their pre-target phase and calculated the HR within a 180° phase window (e.g., 0–180°). We then shifted this phase window by 5° and recalculated the HR (e.g., 5–185°, then 10–190°, etc.), repeating this procedure until we generated phase-detection relationship functions, spanning all phases, for each frequency (Fig. 3C–D). These functions provided the frequency-specific relationship between oscillatory phase and behavioral performance. Hypothesizing a signature shape, with a peak in visual-target detection separated from a trough by approximately 180°, we reduced these functions to a single value for each frequency. Specifically, we applied the fast Fourier transform (FFT) to each function (i.e., at each frequency, from 3–60 Hz) and kept the second component, which represents a one-cycle sine wave (matching the hypothesized shape of our phase-detection relationship functions). The amplitude of this one-cycle, sinusoidal component—determined both by how closely the function approximated a one-cycle sine wave and by the effect size—was used to measure the strength of the phase-detection relationship (Fiebelkorn et al., 2013b). Figure S7 shows the results of the same procedure using 90° phase windows (instead of 180° phase windows). Decreasing the size of the phase windows (from 180° to 90°) increased effect sizes but did not change the pattern of the results.

To test for statistical significance, we (i) shuffled the observed pre-target phase measurements (1500 times) relative to the observed behavioral data (breaking the

relationship between phase and behavioral performance) and (ii) repeated the analysis steps. We then compared the resulting reference distributions (at each frequency) to the magnitude of observed phase-detection relationships (accounting for multiple comparisons).

The present results revealed significant phase-detection relationships across multiple frequency bands (Fig. 3C, D). We next examined whether phase-detection relationships at higher frequencies were dependent on the phase of theta-band activity. Here, we focused on the theta frequencies with the strongest phase-detection relationships: 5 Hz for FEF and 4 Hz for LIP (Fig. 3C, D). We first binned trials into two (180°) theta-phase bins centered on the peaks and troughs of the phase-detection relationships observed during the previous analysis (Fig. 3A, B). We then re-calculated the phase-detection relationships from 9–60 Hz, separately for each theta-phase bin, using the same procedure described above (Fig. 3E, F).

To first establish the independence of theta phase from the phase of higher frequencies, we compared the circular distributions of each of the higher frequencies (from 9 to 60 Hz) when binned by theta (into “good” vs. “poor”), using the Kuiper two-sample test. These tests revealed no significant differences at frequencies greater than 12 Hz, meaning a dependence between theta phase and higher-frequency phases was not an issue for most of the data points presented in Fig. 3E–F, which range from 9–60 Hz. For 9–12 Hz, significant differences between the circular distributions are consistent with leakage between frequencies that results from non-ideal filters. That is, the circular distributions (“good bin” vs. “poor bin”) become increasingly dissimilar at frequencies closer to the binning frequency. If such filtering effects were driving differences in phase-HR relationships (at higher frequencies) between the two theta bins (“good bin” vs. “poor bin”), we would expect to observe a different pattern of results from that observed in Figure 3E–F. That is, we would expect to observe stronger effects closer to the binning frequency that decrease with increasing frequency (i.e., further from the binning frequency), rather than the clear peaks shown in Figure 3E–F.

For this theta-dependent analysis, we tested statistical significance by (i) shuffling the observed pre-target phase estimates (1500 times), separately within each theta-phase bin, relative to the observed behavioral data (breaking the relationship between phase and behavioral performance) and (ii) repeated our analysis steps. We then compared the resulting bin-specific reference distributions (at each higher frequency) to the magnitude of observed bin-specific phase-detection relationships (accounting for multiple comparisons). This approach determined whether there were statistically significant phase-detection relationships (from 9–60 Hz) within each theta-phase bin.

Cross-Frequency Phase-Amplitude Coupling (PAC)—We examined both within- and between-region PAC. We first convolved complex Morlet wavelets with the LFP signal prior to target presentation, using the results to derive phase estimates from 4 to 6 Hz. These theta frequencies were based on significant peaks in the previously measured phase-behavior relationships (Fig. 3C, D). Our final PAC results are averaged across these theta frequencies. We next sorted theta-phase estimates and iteratively calculated average power at higher frequencies (from 9–60 Hz) within 180° phase windows (e.g., 0–180°), shifting the phase window in 5° steps (e.g., 5–185°, then 10–190°, etc.). To aid in visual comparisons across

frequencies (i.e., for Fig. 4A, C), we normalized these phase-power relationships by subtracting and dividing by the average power across all phases (separately for each frequency). Multiplying by 100 revealed the percent modulation in power as a function of theta phase. The steps to this point (i.e., binning power estimates by phase) are similar to other approaches to measuring PAC (Canolty et al., 2006; Jensen and Colgin, 2007; Tort et al., 2010). Next, hypothesizing the same signature shape as phase-detection relationships (i.e., with a peak in power separated from a trough by approximately 180°) we reduced these phase-power functions to a single value for each frequency (Fig. 4B, D). *Specifically, we applied FFTs and kept the second component, which represented the amplitude of an oscillation with a single cycle, matching the hypothesized shape (Fiebelkorn et al., 2013b).*

To test for statistical significance, we (i) shuffled our observed pre-target theta-phase estimates (1500 times) relative to observed higher-frequency power (breaking the relationship between theta phase and higher-frequency power) and (ii) repeated our analysis steps. We then compared the magnitude of resulting reference distributions to the observed PAC (accounting for multiple comparisons).

Because between-condition differences in power (at either the lower or the higher frequency) can lead to spurious differences in PAC (Aru et al., 2015), we conducted a control analysis that equated power between the cued and uncued conditions. We used the ft_stratify function from the FieldTrip toolbox (Donders Institute for Brain, Cognition, and Behaviour), which also equates sample sizes. Stratification involves subsampling the original dataset to equate power, meaning that the results vary somewhat on each run. We therefore ran 1500 iterations of the stratification procedure (separately for PAC in FEF, LIP, FEF/LIP, and LIP/FEF). Figure S9 displays the mean and standard deviation of these power-equating iterations, confirming the between-condition results shown in Figure 4.

For similar reasons (i.e., differences in power can lead to spurious findings), we used the same stratification procedure to verify our between-condition comparisons of synchronization between FEF and LIP (Fig. 5). We equated theta power prior to calculating LFP-LFP phase coupling, spike-LFP phase coupling, and Granger causality. (These synchronization measures are described below.) The results of the control analyses, which are presented in Figure S12, confirm the between-condition findings reported in Figure 5.

We additionally performed a control analysis to test whether theta-dependent changes in oscillatory power (i.e., PAC) were associated with the occurrence of microsaccades. These small, fixational eye movements have previously been linked to theta-band activity in visual cortex (Bosman et al., 2009) and changes in visual processing in FEF (Chen et al., 2015). The eye tracker we initially used to measure eye position had a maximum sampling rate of 240Hz (an Eye-trac 6 from Applied Science Laboratories), but we eventually switched to an eye tracker that had a sampling rate of 1000 Hz (an EyeLink 1000 Plus from SR Research). For the control analysis, we used a subset of recording sessions where eye position was sampled at a high enough rate (i.e., 1000 Hz) to detect microsaccades (N = 30 recording sessions for FEF, N = 32 recording sessions for LIP, N = 22 recordings sessions with matched response fields for FEF and LIP). We defined microsaccades as saccades with amplitudes less than 1° of the visual angle (Engbert and Kliegl, 2003, 2004). Trials with

saccades greater than 1° degree were aborted and subsequently excluded from all analyses. Figure S10 displays PAC for the recording sessions during which we were able to detect the occurrence of microsaccades (i.e., those sessions when we used the EyeLink 1000 Plus to measure eye position), both before and after eliminating trials with microsaccades during the cue-target delay. Removing trials with microsaccades did not substantially change the pattern of the results or alter the statistical significance.

Power-Detection Relationships—For this analysis, our goal was to test whether oscillatory power in the frontoparietal attention network was linked to behavioral performance during spatial attention. We first used the complex results of the Morlet wavelet convolution (see above) to derive pre-target power estimates from 3–60 Hz (in 1-Hz steps). We then (i) binned trials, based on median splits in power, into low- and high-power trials (at each frequency), (ii) calculated HRs in each of those bins, and (iii) took the difference in HRs (Fig. S11A, B).

To test for statistical significance, we (i) shuffled the observed pre-target power estimates (1500 times) relative to the observed behavioral data (breaking the relationship between power and behavioral performance), (ii) redistributed the randomized data between the low- and high-power bins, and (iii) recalculated the HRs. We then compared the resulting reference distributions to the observed differences in HRs (between the low- and high-power bins). Because power-related differences in HRs could be either positive or negative, we compared the observed differences with both tails of the reference distributions, using an alpha criterion of 0.025 (accounting for multiple comparisons).

We next examined power-detection relationships across time (Fig. S11C, D), relative to target presentation, from −500 to 0 ms (in 10-ms steps). Our goal was to determine whether these time-resolved links to behavioral performance demonstrated evidence of theta-band modulation (or periodicity). To this end, we applied FFTs to the time-resolved data (at each frequency, from 15–60 Hz), measuring the strength of theta-band periodicity. When examining the results of these FFTs, we again focused on 5 Hz for FEF and 4 Hz for LIP (i.e., where we previously observed peaks in phase-detection relationships). To determine whether periodicity in the time-resolved data (i.e., power-detection relationships) was statistically significant, we (i) shuffled the data across time (1500 times) and (ii) reapplied our analysis steps (to the randomized data), compiling reference distributions. We then compared the resulting reference distributions with the observed FFT values (accounting for multiple comparisons).

Beta power in both FEF and LIP was predictive of visual-target detection at various time points (relative to target presentation), with the nature of that relationship alternating between (i) windows when increased beta power was associated with better behavioral performance and (ii) windows when increased beta power was associated with worse behavioral performance. These windows (or states) significantly alternated at a frequency in the theta band (permutation test, $p < 0.001$; Fig. S11E, F). The best fit for FEF data occurred at 5 Hz and the best fit for LIP data occurred at 4 Hz. Despite the small difference in the best-fit theta frequency (i.e., 5 Hz vs. 4 Hz), the alternating windows appeared to align across FEF and LIP (e.g., with windows, relative to target presentation, when increased beta

power was associated with better behavioral performance co-occurring in FEF and LIP). These alternating windows reflect an ongoing, periodic process. Beta power is linked to the phase of theta-band activity through PAC (Fig. 4). Therefore, knowing whether beta power is relatively high or low at any given time point is predictive of the temporal dynamics (i.e., theta phase and beta power) that will ultimately occur at target presentation. That is, low beta power at a given time point is associated with better behavioral performance if the ongoing, periodic process will alternate (with theta-band rhythmicity) back to high beta power just prior to target presentation.

LFP-LFP Phase Coupling—We convolved complex Morlet wavelets with LFPs to derive pre-target phase estimates (from 3–8 Hz), limited to trials when the cue-target delay was at least 950 ms. We then used the phase-locking value (Lachaux et al., 1999) to measure between-region phase consistency, including only those recording sessions when FEF and LIP had their strongest responses to stimuli within the same visual quadrant (N = 67). The phase-locking value is defined as follows:

$$PLV = \left| \frac{1}{N} \sum_{n=1}^{N} e^{-i(\varphi_1 - \varphi_2)} \right|,$$

with N being the total number of trials, n being the trial index, and φ_1, φ_2 being the phase measured at electrodes 1 and 2, respectively. PLV is indexed between 1, when the phase difference at the two electrodes is perfectly consistent across trials, and 0 when the phase difference is randomly distributed across trials. A consistent between-region phase relationship is generally thought to reflect strong network connectivity (Figs. 5A, S12A).

We compared PLV between attention conditions (cued location vs. baseline location), using a non-parametric randomization procedure to test for statistical significance. We repeatedly shuffled trials between conditions and re-calculated the difference in PLV (1500 times), generating a reference distribution.

Granger Causality—Here, we used frequency-specific Granger causality to measure the influence of FEF on theta-band activity in LIP relative to the influence of LIP on theta-band activity in FEF, when response fields overlapped the cued location (Figs. 5C, S12C). We first downsampled the data to 250 Hz, subtracted the mean, and then divided by the standard deviation. For MVAR modeling, with the BSMART toolbox for Matlab (Cui et al., 2008), we used a model order of 15, which generally corresponded to the first Akaike information criterion value. The general pattern of results, however, was consistent using model orders at 10, 15, and 20 (we did not test model orders outside of this range).

To establish statistical significance, we used a non-parametric randomization approach, shuffling the trial data and re-calculating Granger causality (1500 times). We then compared the compiled reference distribution of differences between FEF to LIP and LIP to FEF Granger causal influence to the observed values (controlling for multiple comparisons).

Analysis of Neuronal Response Profiles—Neurons in FEF and LIP have previously been classified based on their responses to visual stimuli and during saccadic eye

movements, as visual, visual-movement, and movement types (Barash et al., 1991a, b; Bruce and Goldberg, 1985; Bruce et al., 1985). In the present task, monkeys responded by releasing a lever rather than by making a saccade to the target. We still observed three distinct response profiles: cue-responsive (i.e., those with a significant response to the cue but not the target), cue-target-responsive (i.e., those with a significant response to both the target and the cue), and target-responsive (i.e., those with a significant response to the target but not the cue). We hypothesized that neurons responding to the low-contrast target (but not responding to the much more salient spatial cue) must have a function outside sensory processing. To test whether such neurons might be the same neurons previously associated with saccade-related activity, we utilized trials when the monkeys failed to maintain fixation during the cue-target delay. We time-locked population PSTHs to a trigger associated with these eye-movement errors (Fig. S6). This analysis was limited to a subset of neurons from recording sessions when the monkeys made at least five eye-movement errors, both when the RF was centered on the cued location and when the RF was centered on the uncued location (i.e., the baseline condition). Both cue-target-responsive (N = 26) and target-responsive neurons (N = 12) showed an increasing spike rate leading up to eye movement errors when the RF was centered on the cued location. Cue-responsive neurons (N = 20), on the other hand, showed no such increasing spike rate (but rather a sustained, enhanced spike rate). These data therefore suggest that cue-target-responsive and target-responsive neurons may be identical to the neural response types previously classified as visual-movement and movement neurons.

Previous studies have also shown that only neurons with visual responses (i.e., visual and visual-movement neurons) and not movement neurons are modulated during the cue-target delay under conditions of covert spatial attention (Gregoriou et al., 2012; Thompson et al., 2005). Here, we found a similar pattern of results; with attention-related increases in spike rates restricted to cue- and cue-target-responsive neurons. This pattern of results provides further evidence that cue-target-responsive and target-responsive neurons may correspond to neurons previously classified as visual-movement and movement neurons.

In the present data, the neuron counts for target-responsive neurons was low, particularly for between-region analyses. For example, we only recorded from eight target-responsive neurons in FEF with RFs that simultaneously aligned with response fields in LIP. We therefore limited our response-type-specific analyses to cue-responsive and cue-target-responsive neurons (i.e., those neurons with attention-related effects during the cue-target delay).

Spike-LFP Phase Coupling—We measured the between-region clustering of spike times relative to oscillatory phase in LFPs (e.g., spikes time in FEF relative to oscillatory phase in LIP), from 3–8 Hz. Spike-LFP phase coupling, relative to LFP-LFP phase coupling, avoids spurious coupling attributable to a common reference. For each spike time, we calculated corresponding phase estimates (3–8 Hz) from the LFPs (centered on the spike time), again only using trials when the cue-target delay was at least 950 ms. For this analysis, we used the pairwise phase consistency (PPC), which is not biased by differences in spike counts or trial numbers (Vinck et al., 2010) (http://www.fieldtriptoolbox.org/tutorial/spikefield). For the present study, this was an important consideration, as we compared spike-LFP phase

coupling between conditions with a large difference in the number of total spikes. That is, there was considerably greater spiking activity during the cue-target delay under conditions of spatial attention (i.e., when receptive/response fields overlapped the cued location relative to when receptive/response fields overlapped the uncued location). An acknowledged shortcoming of the PPC measure is that it sometimes results in negative values (Vinck et al., 2010). Here, the error bars reported in Figures 5 and 6 sometimes include negative values, particularly for the uncued condition. However, given large differences in between-condition spike counts, PPC is still our best option for measuring spike-LFP phase coupling.

Stronger clustering of spike times relative to frequency-specific oscillatory phase leads to higher PPC values. For between-region analyses, increased spike-LFP phase coupling (as measured with PPC) is thought to be associated with increased network connectivity. Spikes are typically interpreted as reflecting an output signal, while LFPs are typically interpreted as reflecting an input signal (Pesaran, 2010). Figure 6 shows spike-LFP phase coupling for frequencies from 3–60 Hz.

We compared spike-LFP phase coupling between the cued and uncued locations, separately for neurons with two response profiles: cue-responsive, and cue-target-responsive. See the previous section for a description of these response profiles. To test for statistically significant differences in spike-LFP phase coupling when receptive/response fields were centered on either the cued or the uncued location, we (i) shuffled (1500 times) trials between conditions (cued vs. uncued), and then (ii) recalculated the difference in PPC between the randomized conditions. We then compared the resulting reference distributions with the observed difference in PPC values.

DATA AND SOFTWARE AVAILABILITY

Freely available software and algorithms used for analysis are listed in the resource table. All custom scripts and data contained in this manuscript are available upon request from the Lead Contact: Ian C. Fiebelkorn.

Supplementary Material

Refer to Web version on PubMed Central for supplementary material.

ACKNOWLEDGMENTS

We thank C. E. Schroeder and T. J. Buschman for their insightful comments on the manuscript. This work was supported by a training fellowship to I.C.F. (F32EY023465), and by grants from NIMH (R01MH064063, Silvio O. Conte Center (21560-685) and NEI (RO1EY017699, R21EY023565) to S.K.

REFERENCES

Aru J, Aru J, Priesemann V, Wibral M, Lana L, Pipa G, Singer W, and Vicente R (2015). Untangling cross-frequency coupling in neuroscience. Current opinion in neurobiology 31, 51–61. [PubMed: 25212583]

Barash S, Bracewell RM, Fogassi L, Gnadt JW, and Andersen RA (1991a). Saccade-related activity in the lateral intraparietal area. I. Temporal properties; comparison with area 7a. Journal of neurophysiology 66, 1095–1108. [PubMed: 1753276]

Barash S, Bracewell RM, Fogassi L, Gnadt JW, and Andersen RA (1991). Saccade-related activity in the lateral intraparietal area. II. Spatial properties. Journal of neurophysiology 66, 1109–1124. [PubMed: 1753277]

Bastos AM, Vezoli J, Bosman CA, Schoffelen JM, Oostenveld R, Dowdall JR, De Weerd P, Kennedy H, and Fries P (2015). Visual Areas Exert Feedforward and Feedback Influences through Distinct Frequency Channels. Neuron 85, 390–401. [PubMed: 25556836]

Benedetto A, and Morrone MC (2017). Saccadic Suppression Is Embedded Within Extended Oscillatory Modulation of Sensitivity. The Journal of neuroscience : the official journal of the Society for Neuroscience 37, 3661–3670. [PubMed: 28270573]

Berg RW, and Kleinfeld D (2003). Rhythmic whisking by rat: retraction as well as protraction of the vibrissae is under active muscular control. Journal of neurophysiology 89, 104–117. [PubMed: 12522163]

Bichot NP, Rossi AF, and Desimone R (2005). Parallel and serial neural mechanisms for visual search in macaque area V4. Science 308, 529–534. [PubMed: 15845848]

Bisley JW, and Goldberg ME (2010). Attention, intention, and priority in the parietal lobe. Annual review of neuroscience 33, 1–21.

Bollimunta A, Chen Y, Schroeder CE, and Ding M (2008). Neuronal mechanisms of cortical alpha oscillations in awake-behaving macaques. The Journal of neuroscience : the official journal of the Society for Neuroscience 28, 9976–9988. [PubMed: 18829955]

Bollimunta A, Mo J, Schroeder CE, and Ding M (2011). Neuronal mechanisms and attentional modulation of corticothalamic alpha oscillations. The Journal of neuroscience : the official journal of the Society for Neuroscience 31, 4935–4943. [PubMed: 21451032]

Bosman CA, Schoffelen JM, Brunet N, Oostenveld R, Bastos AM, Womelsdorf T, Rubehn B, Stieglitz T, De Weerd P, and Fries P (2012). Attentional stimulus selection through selective synchronization between monkey visual areas. Neuron 75, 875–888. [PubMed: 22958827]

Bosman CA, Womelsdorf T, Desimone R, and Fries P (2009). A microsaccadic rhythm modulates gamma-band synchronization and behavior. The Journal of neuroscience : the official journal of the Society for Neuroscience 29, 9471–9480. [PubMed: 19641110]

Bruce CJ, and Goldberg ME (1985). Primate frontal eye fields. I. Single neurons discharging before saccades. Journal of neurophysiology 53, 603–635. [PubMed: 3981231]

Bruce CJ, Goldberg ME, Bushnell MC, and Stanton GB (1985). Primate frontal eye fields. II. Physiological and anatomical correlates of electrically evoked eye movements. Journal of neurophysiology 54, 714–734. [PubMed: 4045546]

Buffalo EA, Fries P, Landman R, Buschman TJ, and Desimone R (2011). Laminar differences in gamma and alpha coherence in the ventral stream. Proceedings of the National Academy of Sciences of the United States of America 108, 11262–11267. [PubMed: 21690410]

Busch NA, and VanRullen R (2010). Spontaneous EEG oscillations reveal periodic sampling of visual attention. Proceedings of the National Academy of Sciences of the United States of America 107, 16048–16053. [PubMed: 20805482]

Buschman TJ, and Miller EK (2007). Top-down versus bottom-up control of attention in the prefrontal and posterior parietal cortices. Science 315, 1860–1862. [PubMed: 17395832]

Buschman TJ, and Miller EK (2009). Serial, covert shifts of attention during visual search are reflected by the frontal eye fields and correlated with population oscillations. Neuron 63, 386–396. [PubMed: 19679077]

Canolty RT, and Knight RT (2010). The functional role of cross-frequency coupling. Trends in cognitive sciences 14, 506–515. [PubMed: 20932795]

Chen CY, Ignashchenkova A, Thier P, and Hafed ZM (2015). Neuronal Response Gain Enhancement prior to Microsaccades. Current biology : CB 25, 2065–2074. [PubMed: 26190072]

Colgin LL (2013). Mechanisms and functions of theta rhythms. Annual review of neuroscience 36, 295–312.

Corbetta M, Akbudak E, Conturo TE, Snyder AZ, Ollinger JM, Drury HA, Linenweber MR, Petersen SE, Raichle ME, Van Essen DC, and Shulman GL (1998). A common network of functional areas for attention and eye movements. Neuron 21, 761–773. [PubMed: 9808463]

Cox RW (1996). AFNI: software for analysis and visualization of functional magnetic resonance neuroimages. Computers and biomedical research, an international journal 29, 162–173.

Cui J, Xu L, Bressler SL, Ding M, and Liang H (2008). BSMART: a Matlab/C toolbox for analysis of multichannel neural time series. Neural networks : the official journal of the International Neural Network Society 21, 1094–1104. [PubMed: 18599267]

Dugue L, Marque P, and VanRullen R (2015). Theta oscillations modulate attentional search performance periodically. Journal of cognitive neuroscience 27, 945–958. [PubMed: 25390199]

Dugue L, Roberts M, and Carrasco M (2016). Attention Reorients Periodically. Current biology : CB 26, 1595–1601. [PubMed: 27265395]

Egly R, Driver J, and Rafal RD (1994). Shifting visual attention between objects and locations: evidence from normal and parietal lesion subjects. Journal of experimental psychology General 123, 161–177. [PubMed: 8014611]

Engbert R, and Kliegl R (2003). Microsaccades uncover the orientation of covert attention. Vision research 43, 1035–1045. [PubMed: 12676246]

Engbert R, and Kliegl R (2004). Microsaccades keep the eyes' balance during fixation. Psychological science 15, 431–436. [PubMed: 15147499]

Esghaei M, Daliri MR, and Treue S (2015). Attention Decreases Phase-Amplitude Coupling, Enhancing Stimulus Discriminability in Cortical Area MT. Frontiers in neural circuits 9, 82. [PubMed: 26733820]

Fanselow EE, and Nicolelis MA (1999). Behavioral modulation of tactile responses in the rat somatosensory system. The Journal of neuroscience : the official journal of the Society for Neuroscience 19, 7603–7616. [PubMed: 10460266]

Fecteau JH, and Munoz DP (2006). Salience, relevance, and firing: a priority map for target selection. Trends in cognitive sciences 10, 382–390. [PubMed: 16843702]

Fiebelkorn IC, Foxe JJ, Butler JS, Mercier MR, Snyder AC, and Molholm S (2011). Ready, set, reset: stimulus-locked periodicity in behavioral performance demonstrates the consequences of cross-sensory phase reset. The Journal of neuroscience : the official journal of the Society for Neuroscience 31, 9971–9981. [PubMed: 21734288]

Fiebelkorn IC, Saalmann YB, and Kastner S (2013a). Rhythmic sampling within and between objects despite sustained attention at a cued location. Current biology : CB 23, 2553–2558. [PubMed: 24316204]

Fiebelkorn IC, Snyder AC, Mercier MR, Butler JS, Molholm S, and Foxe JJ (2013b). Cortical cross-frequency coupling predicts perceptual outcomes. NeuroImage 69, 126–137. [PubMed: 23186917]

Fries P (2015). Rhythms for Cognition: Communication through Coherence. Neuron 88, 220–235. [PubMed: 26447583]

Fries P, Reynolds JH, Rorie AE, and Desimone R (2001). Modulation of oscillatory neuronal synchronization by selective visual attention. Science 291, 1560–1563. [PubMed: 11222864]

Ganguly K, and Kleinfeld D (2004). Goal-directed whisking increases phase-locking between vibrissa movement and electrical activity in primary sensory cortex in rat. Proceedings of the National Academy of Sciences of the United States of America 101, 12348–12353. [PubMed: 15297618]

Gregoriou GG, Gotts SJ, and Desimone R (2012). Cell-type-specific synchronization of neural activity in FEF with V4 during attention. Neuron 73, 581–594. [PubMed: 22325208]

Gregoriou GG, Gotts SJ, Zhou H, and Desimone R (2009). High-frequency, long-range coupling between prefrontal and visual cortex during attention. Science 324, 1207–1210. [PubMed: 19478185]

Haegens S, Nacher V, Luna R, Romo R, and Jensen O (2011). alpha-Oscillations in the monkey sensorimotor network influence discrimination performance by rhythmical inhibition of neuronal spiking. Proceedings of the National Academy of Sciences of the United States of America 108, 19377–19382. [PubMed: 22084106]

Helfrich RF, Fiebelkorn IC, Szczepanski SM, Lin JJ, Parvizi J, Knight RT, and Kastner S (2018). Neural mechanisms of sustained attention are rhythmic. Neuron.

Hogendoorn H (2016). Voluntary Saccadic Eye Movements Ride the Attentional Rhythm. Journal of cognitive neuroscience 28, 1625–1635. [PubMed: 27243615]

Jarvis MR, and Mitra PP (2001). Sampling properties of the spectrum and coherency of sequences of action potentials. Neural computation 13, 717–749. [PubMed: 11255566]

Jenkinson M, Beckmann CF, Behrens TE, Woolrich MW, and Smith SM (2012). Fsl. NeuroImage 62, 782–790. [PubMed: 21979382]

Jensen O, and Colgin LL (2007). Cross-frequency coupling between neuronal oscillations. Trends in cognitive sciences 11, 267–269. [PubMed: 17548233]

Kelly SP, Lalor EC, Reilly RB, and Foxe JJ (2006). Increases in alpha oscillatory power reflect an active retinotopic mechanism for distracter suppression during sustained visuospatial attention. Journal of neurophysiology 95, 3844–3851. [PubMed: 16571739]

Kienitz R, Schmiedt JT, Shapcott KA, Kouroupaki K, Saunders RC, and Schmid MC (2018). Theta rhythmic neuronal activity and reaction times arising from cortical receptive field interactions during distributed attention. Current Biology, 10.1016/j.cub.2018.05.086.

Killian NJ, Jutras MJ, and Buffalo EA (2012). A map of visual space in the primate entorhinal cortex. Nature 491, 761–764. [PubMed: 23103863]

Lachaux JP, Rodriguez E, Martinerie J, and Varela FJ (1999). Measuring phase synchrony in brain signals. Human brain mapping 8, 194–208. [PubMed: 10619414]

Lakatos P, Karmos G, Mehta AD, Ulbert I, and Schroeder CE (2008). Entrainment of neuronal oscillations as a mechanism of attentional selection. Science 320, 110–113. [PubMed: 18388295]

Landau AN, and Fries P (2012). Attention samples stimuli rhythmically. Current biology : CB 22, 1000–1004. [PubMed: 22633805]

Landau AN, Schreyer HM, van Pelt S, and Fries P (2015). Distributed Attention Is Implemented through Theta-Rhythmic Gamma Modulation. Current biology : CB 25, 2332–2337. [PubMed: 26279231]

Liebe S, Hoerzer GM, Logothetis NK, and Rainer G (2012). Theta coupling between V4 and prefrontal cortex predicts visual short-term memory performance. Nature neuroscience 15, 456–462, S451–452. [PubMed: 22286175]

Lisman JE, and Jensen O (2013). The theta-gamma neural code. Neuron 77, 1002–1016. [PubMed: 23522038]

Makeig S, Westerfield M, Jung TP, Enghoff S, Townsend J, Courchesne E, and Sejnowski TJ (2002). Dynamic brain sources of visual evoked responses. Science 295, 690–694. [PubMed: 11809976]

Manning JR, Jacobs J, Fried I, and Kahana MJ (2009). Broadband Shifts in Local Field Potential Power Spectra Are Correlated with Single-Neuron Spiking in Humans. Journal of Neuroscience 29, 13613–13620. [PubMed: 19864573]

Miller KJ, Leuthardt EC, Schalk G, Rao RP, Anderson NR, Moran DW, Miller JW, and Ojemann JG (2007). Spectral changes in cortical surface potentials during motor movement. The Journal of neuroscience : the official journal of the Society for Neuroscience 27, 2424–2432. [PubMed: 17329441]

Moran J, and Desimone R (1985). Selective attention gates visual processing in the extrastriate cortex. Science 229, 782–784. [PubMed: 4023713]

Moser EI, Kropff E, and Moser MB (2008). Place cells, grid cells, and the brain's spatial representation system. Annual review of neuroscience 31, 69–89.

Moldakarimov S, Rollenhagen JE, Olson CR, and Chow CC (2005). Competitive dynamics in cortical responses to visual stimuli. Journal of Neurophysiology 94, 3388–3396. [PubMed: 15944239]

Oostenveld R, Fries P, Maris E, and Schoffelen JM (2011). FieldTrip: Open source software for advanced analysis of MEG, EEG, and invasive electrophysiological data. Computational intelligence and neuroscience 2011, 156869. [PubMed: 21253357]

Otero-Millan J, Troncoso XG, Macknik SL, Serrano-Pedraza I, and Martinez-Conde S (2008). Saccades and microsaccades during visual fixation, exploration, and search: foundations for a common saccadic generator. Journal of vision 8, 21 21–18.

Pesaran B (2010). Neural correlations, decisions, and actions. Current opinion in neurobiology 20, 166–171. [PubMed: 20359885]

Phillips JM, Vinck M, Everling S, and Womelsdorf T (2014). A long-range fronto-parietal 5- to 10-Hz network predicts "top-down" controlled guidance in a task-switch paradigm. Cerebral cortex 24, 1996–2008. [PubMed: 23448872]

Pigarev IN, Saalmann YB, and Vidyasagar TR (2009). A minimally invasive and reversible system for chronic recordings from multiple brain sites in macaque monkeys. Journal of neuroscience methods 181, 151–158. [PubMed: 19422856]

Pogosyan A, Gaynor LD, Eusebio A, and Brown P (2009). Boosting cortical activity at Beta-band frequencies slows movement in humans. Current biology : CB 19, 1637–1641. [PubMed: 19800236]

Posner MI (1980). Orienting of attention. The Quarterly journal of experimental psychology 32, 3–25. [PubMed: 7367577]

Posner MI, Rafal RD, Choate LS, and Vaughan J (1985). Inhibition of Return - Neural Basis and Function. Cognitive Neuropsych 2, 211–228.

Reveley C, Gruslys A, Ye FQ, Glen D, Samaha J, B ER, Saad Z, A KS, Leopold DA, and Saleem KS (2017). Three-Dimensional Digital Template Atlas of the Macaque Brain. Cerebral cortex 27, 4463–4477. [PubMed: 27566980]

Rollenhagen JE, and Olson CR (2005). Low-frequency oscillations arising from competitive interactions between visaul stimuli in macaque inferotemporal cortex. Journal of Neurophysiology 94, 3368–3387. [PubMed: 15928064]

Saleem KS, and Logothetis N (2007). A combined MRI and histology atlas of the rhesus monkey brain in stereotaxic coordinates (London ; Burlington, MA: Academic).

Saalmann YB, and Kastner S (2011). Cognitive and perceptual functions of the visual thalamus. Neuron 71, 209–223. [PubMed: 21791281]

Schroeder CE, and Lakatos P (2009). Low-frequency neuronal oscillations as instruments of sensory selection. Trends in neurosciences 32, 9–18. [PubMed: 19012975]

Schroeder CE, Wilson DA, Radman T, Scharfman H, and Lakatos P (2010). Dynamics of Active Sensing and perceptual selection. Current opinion in neurobiology 20, 172–176. [PubMed: 20307966]

Sellers KK, Yu C, Zhou ZC, Stitt I, Li Y, Radtke-Schuller S, Alagapan S, and Frohlich F (2016). Oscillatory Dynamics in the Frontoparietal Attention Network during Sustained Attention in the Ferret. Cell reports 16, 2864–2874. [PubMed: 27626658]

Siegel M, Warden MR, and Miller EK (2009). Phase-dependent neuronal coding of objects in short-term memory. Proceedings of the National Academy of Sciences of the United States of America 106, 21341–21346. [PubMed: 19926847]

Smith SM (2002). Fast robust automated brain extraction. Human brain mapping 17, 143–155. [PubMed: 12391568]

Song K, Meng M, Chen L, Zhou K, and Luo H (2014). Behavioral oscillations in attention: rhythmic alpha pulses mediated through theta band. The Journal of neuroscience : the official journal of the Society for Neuroscience 34, 4837–4844. [PubMed: 24695703]

Spyropoulos G, Bosman C, and Fries P (2018). A Theta Rhythm In Awake Macaque V1 And V4 And Its Attentional Modulation. Proceedings of the National Academy of Sciences of the United States of America 115, E5614–E5623. [PubMed: 29848632]

Squire RF, Noudoost B, Schafer RJ, and Moore T (2013). Prefrontal contributions to visual selective attention. Annual review of neuroscience 36, 451–466.

Szczepanski SM, Crone NE, Kuperman RA, Auguste KI, Parvizi J, and Knight RT (2014). Dynamic changes in phase-amplitude coupling facilitate spatial attention control in fronto-parietal cortex. PLoS biology 12, e1001936. [PubMed: 25157678]

Thompson KG, Biscoe KL, and Sato TR (2005). Neuronal basis of covert spatial attention in the frontal eye field. The Journal of neuroscience : the official journal of the Society for Neuroscience 25, 9479–9487. [PubMed: 16221858]

Tort AB, Komorowski R, Eichenbaum H, and Kopell N (2010). Measuring phase-amplitude coupling between neuronal oscillations of different frequencies. Journal of neurophysiology 104, 1195–1210. [PubMed: 20463205]

van Kerkoerle T, Self MW, Dagnino B, Gariel-Mathis MA, Poort J, van der Togt C, and Roelfsema PR (2014). Alpha and gamma oscillations characterize feedback and feedforward processing in monkey visual cortex. Proceedings of the National Academy of Sciences of the United States of America 111, 14332–14341. [PubMed: 25205811]

VanRullen R, Carlson T, and Cavanagh P (2007). The blinking spotlight of attention. Proceedings of the National Academy of Sciences of the United States of America 104, 19204–19209. [PubMed: 18042716]

VanRullen R (2016). Perceptual Cycles. Trends in cognitive sciences 20, 723–735. [PubMed: 27567317]

Vinck M, van Wingerden M, Womelsdorf T, Fries P, and Pennartz CM (2010). The pairwise phase consistency: a bias-free measure of rhythmic neuronal synchronization. NeuroImage 51, 112–122. [PubMed: 20114076]

Womelsdorf T, Fries P, Mitra PP, and Desimone R (2006). Gamma-band synchronization in visual cortex predicts speed of change detection. Nature 439, 733–736. [PubMed: 16372022]

Worden MS, Foxe JJ, Wang N, and Simpson GV (2000). Anticipatory biasing of visuospatial attention indexed by retinotopically specific alpha-band electroencephalography increases over occipital cortex. The Journal of neuroscience : the official journal of the Society for Neuroscience 20, RC63. [PubMed: 10704517]

Wutz A, Muschter E, van Koningsbruggen MG, Weisz N, and Melcher D (2016). Temporal Integration Windows in Neural Processing and Perception Aligned to Saccadic Eye Movements. Current biology : CB 26, 1659–1668. [PubMed: 27291050]

Zhang Y, Chen Y, Bressler SL, and Ding M (2008). Response preparation and inhibition: the role of the cortical sensorimotor beta rhythm. Neuroscience 156, 238–246. [PubMed: 18674598]

HIGHLIGHTS

- Non-human primates, like humans, sample the visual scene in rhythmic cycles.
- Neural oscillations in the frontoparietal network modulate perceptual sensitivity.
- Theta phase acts as a clocking mechanism, organizing alternating attentional states.
- Temporal dynamics linked to specific function and cell type define attentional state.

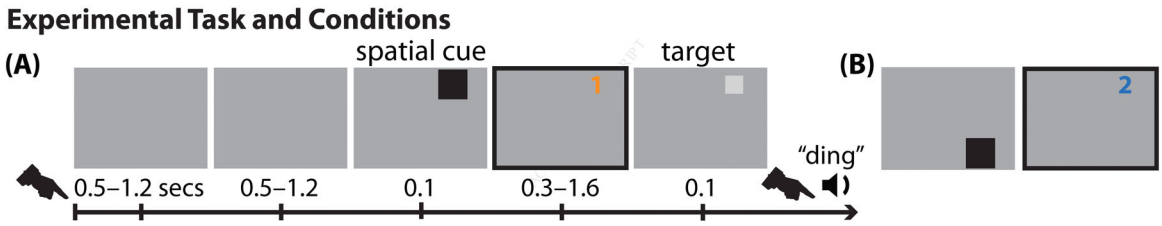

Figure 1. Experimental task.

(A, B) A variant of the Egly-Driver task (Egly et al., 1994), investigating behavioral and electrophysiological responses at (1) a cued location and (2) an uncued location, positioned on a second object.

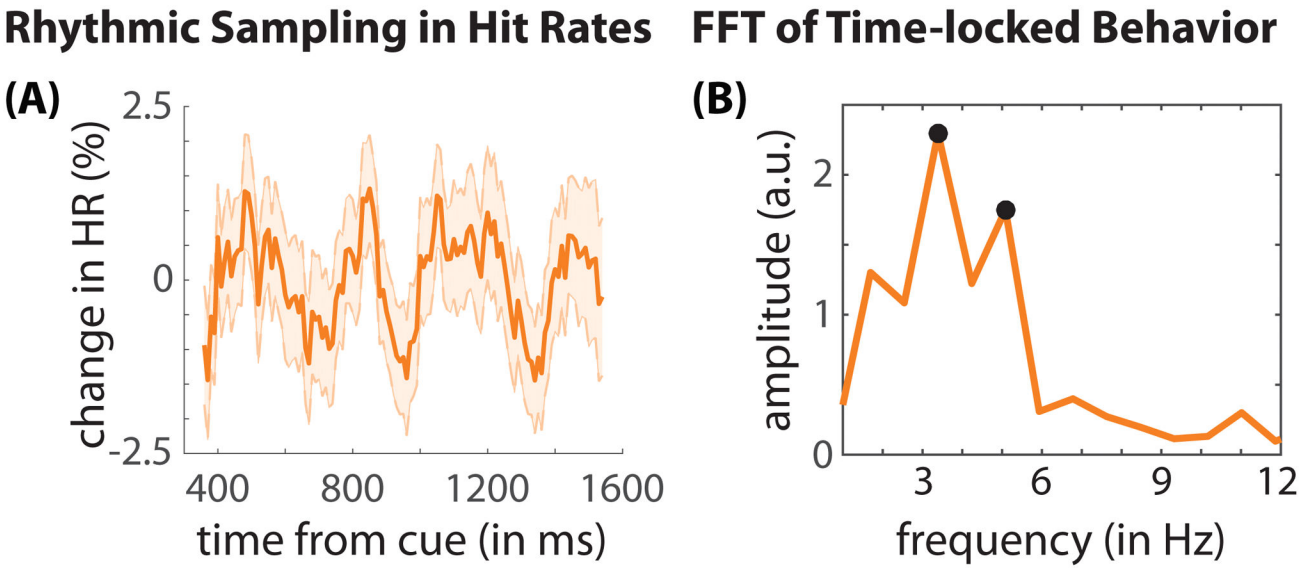

Figure 2. Evidence of rhythmic sampling in monkey behavioral data.

(A) Displays the change in hit rates (HRs) at the cued location as a function of the time from cue (i.e., at different cue-target delays). Behavioral data were compiled across all recording sessions from two monkeys. These data have been linearly detrended, aiding visualization of the periodic effects (see Fig. S2 for the behavioral times-series data prior to detrending). The shaded regions around the lines represent standard error of the mean. **(B)** The fast Fourier transform (FFT) was then used to convert behavioral time-series data into the frequency domain (Fiebelkorn et al., 2011; Fiebelkorn et al., 2013a). The black dots represent statistically significant peaks after corrections for multiple comparisons, demonstrating significant theta-band rhythmicity in monkey behavioral performance.

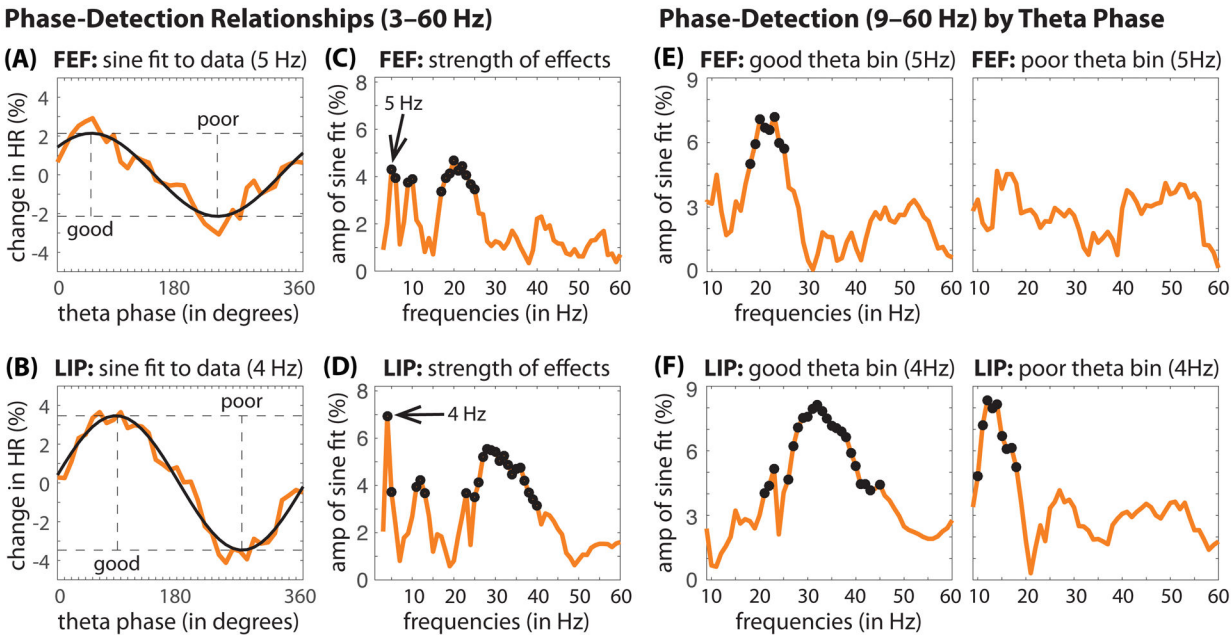

Figure 3. Theta-band activity within the frontoparietal network shapes behavioral performance.

(A, B) The change in hit rate (HR) at the cued location (i.e., when response fields overlapped the cued location) as a function of theta phase. If detectability is dependent on oscillatory phase, HRs binned by phase (in orange) should approximate a one-cycle sine wave (i.e., peaks in visual-target detection should be separated from troughs by approximately 180 degrees). A fast Fourier transform was therefore used to extract a one-cycle, sinusoidal component (in black). The strength of the phase-detection relationship at each frequency, **(C, D)** from 3–60 Hz, was measured as the amplitude of this sinusoidal component (Fiebelkorn et al., 2013b). The black dots represent statistically significant findings after corrections for multiple comparisons. (E, F) Trials were then split into two bins based on theta phase: (i) a bin centered on the theta phase associated with relatively better ("good") behavioral performance and (ii) a bin centered on the theta phase associated with relatively worse ("poor") behavioral performance. Theta-dependent phase-detection relationships were then calculated within each of those bins, from 9–60 Hz. HRs at the cued location are dependent on the phase of neural oscillatory activity in both FEF (97 recording sessions) and LIP (98 recording sessions).

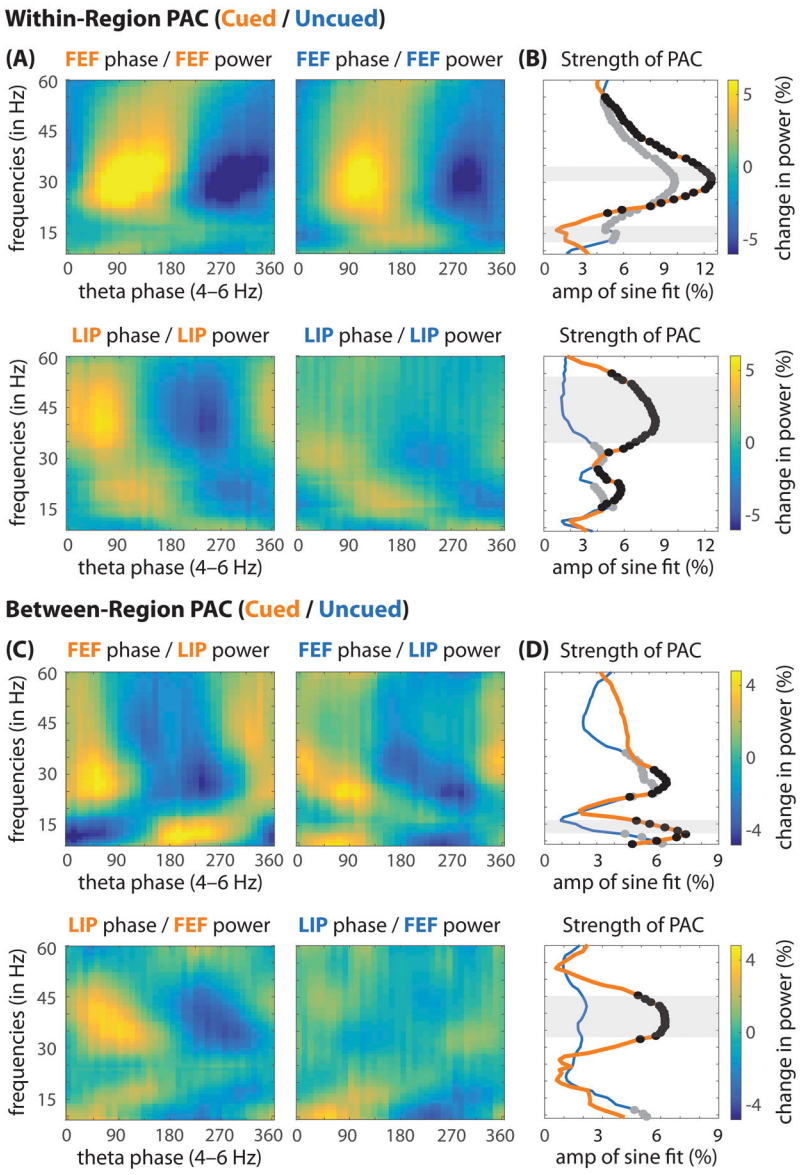

Figure 4. Theta phase in the frontoparietal network modulates higher-frequency power.

All plots show the percent change in power (relative to the mean power at each frequency, from 9–60 Hz), as a function of theta phase. **(A, B)** Within-region phase-amplitude coupling (PAC), between theta phase and higher-frequency power, when response fields overlapped either the cued (orange) or the uncued (blue) location. **(B)** The strength of this coupling was measured by using the fast Fourier transform to extract the amplitude of a one-cycle, sinusoidal component (Fig. 3A, *B).* The black (cued location) and gray (uncued location) dots represent statistically significant PAC after corrections for multiple comparisons. The shaded regions represent statistically significant differences in PAC between the cued and uncued conditions. **(C, D)** Between-region PAC (67 recording sessions with matching response fields in FEF and LIP), again linking theta phase and higher-frequency power.

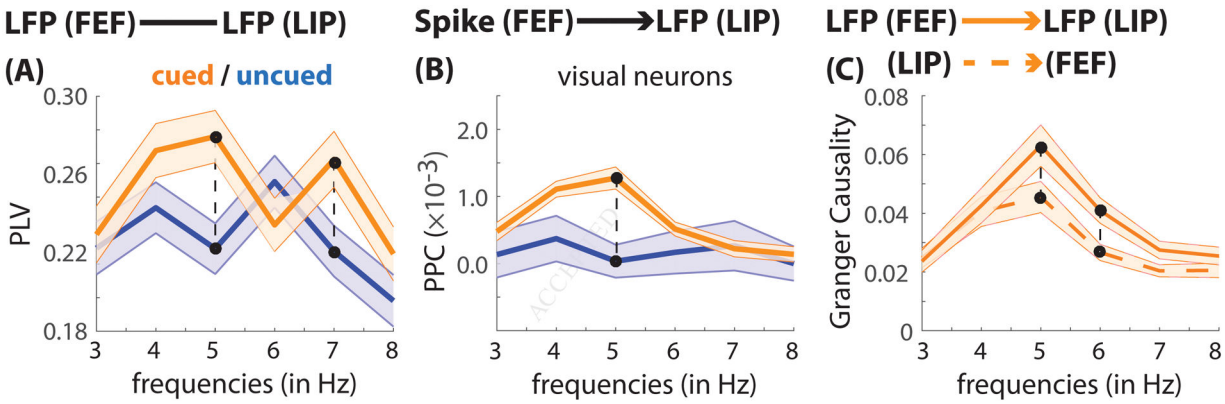

Figure 5. Between-region coupling demonstrates theta-band connectivity in the frontoparietal network.

(A) LFP-LFP phase coupling (measured by the phase-locking value [PLV]) when response fields overlapped either the cued (orange) or the uncued (blue) location. **(B)** Spike-LFP phase coupling (measured by the pairwise phase consistency [PPC]) for visual neurons (N = 36). Spikes in FEF were correlated with oscillatory phase in LIP. **(C)** Granger causal influence when response fields overlapped the cued location (i.e., under conditions of spatial attention), from FEF to LIP (dashed orange) and from LIP to FEF (solid orange). The shaded regions around the lines represent standard error of the mean. The connected black dots represent statistically significant, between-condition findings after corrections for multiple comparisons.

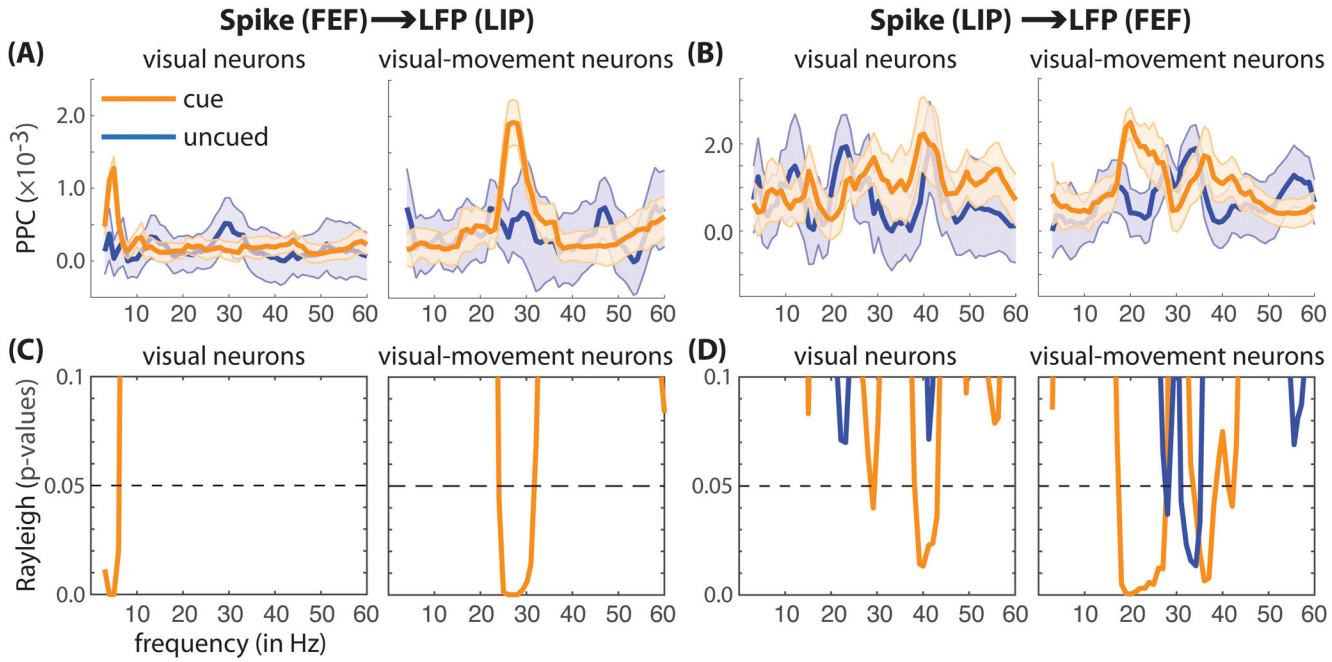

Figure 6. Between-region spike-LFP phase coupling (from 3–60 Hz) when either the cued or uncued location fell within the receptive/response fields, by cell type.

(A) Spikes in FEF were correlated with oscillatory phase (as measured using LFPs) in LIP (using the pairwise phase consistency [PPC]), and **(B)** spikes in LIP were correlated with oscillatory phase in FEF. These results are shown separately for visual and visual-movement neurons. Shaded regions around lines represent SEs. **(C, D)** The results of Rayleigh tests for non-uniformity of spike times relative to oscillatory phase (by condition and cell type). **(C)** Spikes in FEF were significantly coupled to theta-band (cue-responsive neurons) and beta-band (cue-target-responsive neurons) oscillations in LIP during spatial attention. There was no significant spike-LFP phase coupling outside the focus of spatial attention (i.e., at the uncued location). **(D)** Spikes in LIP were significantly coupled to beta-band (cue-target-responsive neurons) and gamma-band (cue-responsive and cue-target responsive neurons) oscillations in FEF during spatial attention. There was also significant spike-LFP phase coupling in the gamma band (cue-target-responsive neurons) outside the focus of spatial attention (i.e., at the uncued location).

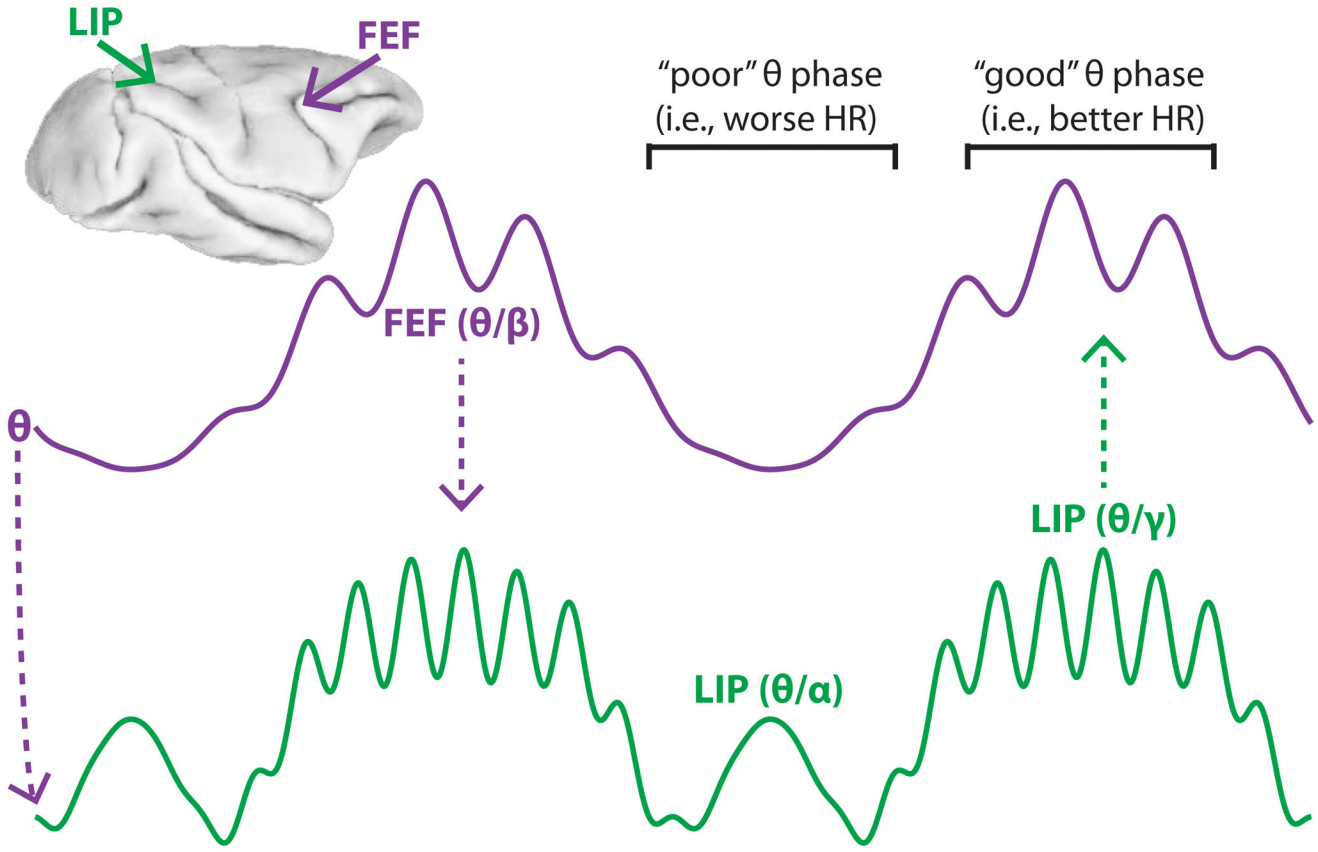

Figure 7. A schematic representing a neural basis of rhythmic sampling during spatial attention.

Theta (3–8 Hz) phase organizes neural activity in the frontoparietal network into two rhythmically alternating attentional states. The first state is characterized by (i) an FEF-dominated, spatially non-specific boost in beta-band activity (16–35 Hz), associated with suppressed attentional shifts, and (ii) an LIP-dominated, spatially specific boost in gamma-band activity (> 35 Hz), associated with enhanced visual processing and better behavioral performance at the cued location. The second state is characterized by a spatially specific boost in LIP-specific alpha-band activity (9–15 Hz), associated with attenuated visual processing and worse behavioral performance at the cued location.